The Pennsylvania State University

The Graduate School

College of Engineering

ELECTRICAL DETECTION OF BIO-MOLECULAR INTERACTIONS USING NANOMETER-SCALE GAP ELECTRODE STRUCTURES

A Thesis in

Engineering Science and Mechanics

by

Joseph Dennis Cuiffi

Submitted in Partial Fulfillment
of the Requirements
for the Degree of

Doctor of Philosophy

May 2004

The thesis of Joseph Dennis Cuiffi was reviewed and approved* by the following:

Stephen J. Fonash
Kunkle Chair Professor of Engineering Science and Mechanics
Thesis Advisor
Chair of Committee

Osama O. Awadelkarim
Professor of Engineering Science and Mechanics

Ayusman Sen
Professor of Chemistry

Mirna Urquidi-Macdonald
Professor of Engineering Science and Mechanics

Judith A. Todd
Professor of Engineering Science and Mechanics
Head of the Department of Engineering Science and Mechanics

*Signatures are on file in the Graduate School

ABSTRACT

Detecting biological molecules faster and with greater sensitivity has immediate impact on medicine and healthcare. Disease identification and drug development rely on the ability to detect and identify biological chemicals and their interactions. Currently, most detection techniques rely on optical methods such as a color change to determine the presence of a biological compound. The ability to perform these tests electrically has the potential for faster and more sensitive results and the ability to couple easily with computer analysis.

A unique sensor device and technique for detecting biological molecules has been developed. Here, an electrical sensor with nanometer-scale dimensions is made using standard processes and equipment found in the semiconductor industry. This sensor has the ability to be chemically modified to detect specific biological compounds. This is the first time a device combining these properties effectively for commercial use has been presented. Processes used in the fabrication of the device are shown to be critical in preserving the ability for chemical modification as a sensor.

A unique chemical linking method has also been developed which allows effective biological modification of the device. This modification of the device allows for specific biological molecules to interact with surfaces of the device. The modification can be used to tailor the device to interact with a range of biological molecules including DNA, proteins and other small bio-molecules. The ability of the chemistry to interact with a variety of different species is important

for commercialization, because a versatile platform is more economically viable to develop.

Using an example system, this device electrically detected the interaction of two biological molecules. The detection scheme makes the use of biologically modified gold nano-particles, which change the electrical characteristics of the device. The sensitivity of the device is among the highest reported for electrical techniques, and the technique itself appears robust enough for commercial development.

Overall, this unique and cost-effective sensor offers sensitive detection of biological molecules.

TABLE OF CONTENTS

LIST OF FIGURES

LIST OF TABLES

ACKNOWLEDGEMENTS

This thesis and the completion of my graduate studies were made possible by my friend and advisor Dr. Stephen J. Fonash. Steve gave me the chance to pursue higher education and provided endless guidance and support.

I also owe thanks to the staff and graduate students at the Penn State Nanofabrication facility for their useful discussions and technical help.

To my parents, I am most grateful. They have supported me throughout my educational studies and my career.

Finally, I would like to thank Glorita for sticking it through the tough times with me, and for this I am forever in her debt.

Chapter 1

Introduction

Studying the interactions and functions of biological molecules enhances our fundamental knowledge of biological systems and ultimately provides the ability to understand and impact medicine and healthcare. Biological systems are extremely complex, and our knowledge of the inner workings of higher-level organisms, which are composed of many such biological systems, is understandably limited. Nevertheless, modern equipment and techniques are creating vast amounts of information in this realm and thereby rapidly advancing the forefront of technological capabilities and understanding of biological systems. This thesis is a contribution to that advancement. It presents a unique sensor technology for the electrical detection of biological molecular interactions, aiming to improve current techniques and ultimately to make them more economically viable for clinical applications. Prior to describing the general approach and goals of this research, this chapter will provide a quick review of important biological molecules, current techniques commonly used in bio-molecular assays and a review of recent research findings in the specific field of electrical detection of biological molecules.

1.1 Important Bio-Molecules and Background of Bio-Molecular Assays

Biological systems are built upon and controlled by several classes of molecules including: ribonucleic acids (DNA and RNA), proteins, lipids and fats, small organic molecules, complex inorganic/organic mixtures (bone) and others. These molecules interact with each other in a variety of ways, most of which may be classified using the fundamental bonding distinctions of hydrogen, ionic, covalent, and Van der Waals bonding along with hydrophobic and hydrophilic interactions (an extension of hydrogen bonding in water). Molecules such as DNA and proteins are large, complex biopolymers that form specific shapes and have specific chemistries that interact with other species. These molecules are the focus of most biochemical assays. Because of their relevance to this research, a quick review of their structure and analysis is provided below.

1.1.1 DNA Structure and Analysis

DNA is a commonly recognized biological molecule. DNA is essentially a sugar (ribose) - phosphate polymer with four possible groups (bases) attached to each ribose group: adenine (A), guanine (G), cytosine (C), and thymine (T). The sequence of each of these groups within the polymer is hardly arbitrary, for it encodes an organism's genetic blueprint, including even the blueprints for its own replication. For purposes of copying and reproducing DNA, two copies of the genetic code are present in each cell. Each copy is an exact inverse of the other, substituting a T for an A and a G for a C. These two inverse strands are referred

to as “complementary”. The strong hydrogen bonding between the C-G and T-A of the opposing and complementary strands cause the DNA to “zip” together and twist into a double-helix shape, first recognized by Watson and Crick. The process by which two single strands of DNA bind together is called hybridization. A schematic of DNA structure is shown in Figure **1-1**.

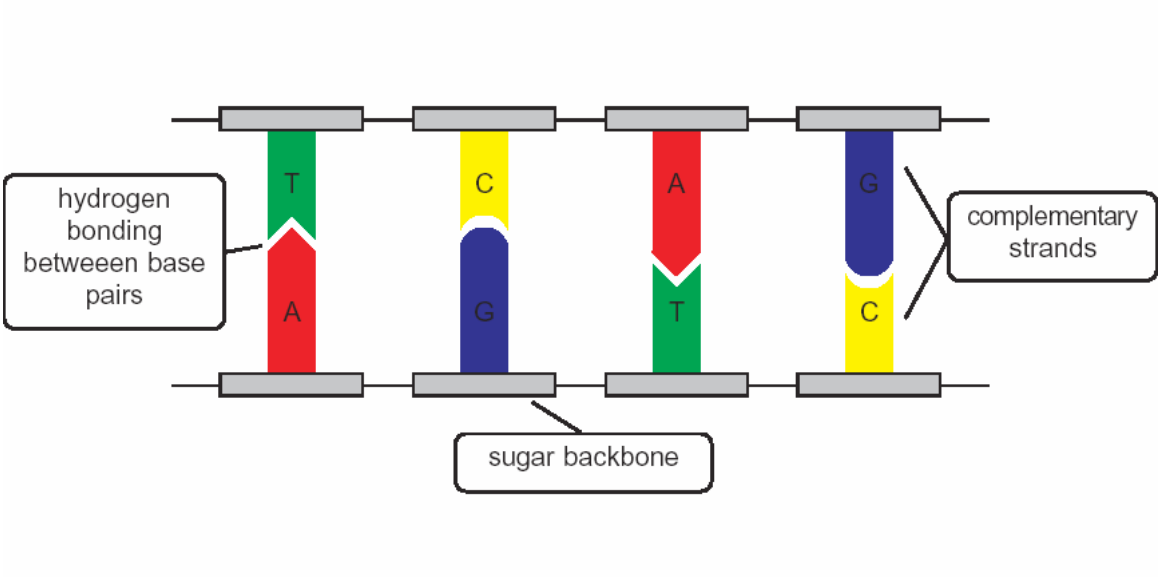

Figure **1-1**: Schematic structure of hybridized, complementary strands of DNA held together by hydrogen bonding.

Although modern medicine cannot yet make full use of the vast amount of information provided in someone’s DNA sequence (or genome), there is an intense drive to improve the sequencing or identification of fragments of DNA by making this process faster and cheaper. Having DNA sequence information can determine genetic disease, identify cancer, and identify people as in forensics. Soon, people will have their DNA genome sequenced at birth, and clinicians will use it as a master reference of ones body. Whether or not we will be able to

effectively change someone's genome or prevent the diseases inherently encoded within their genome, is a long-term question. However, DNA analysis currently has a large commercial market space ranging from forensic fingerprinting to cancer identification and research.

DNA analysis ranges from obtaining its entire sequence, such as in the genome project, or to simply identifying key region markers as in forensic fingerprinting. For the purposes of the research presented in this thesis, it is necessary to understand an analysis technique known as a DNA hybridization experiment. In general, a DNA hybridization experiment uses known single strands of DNA (probes) to determine the sequence of an unknown single strand (target). The experimenter matches the unknown single strand of DNA with its complement (one of the known pieces) through hybridization to form a double stranded DNA as described above. Because of the extreme selectivity in the hydrogen bonding of bases, even single base pair mismatches will prevent hybridization. A key aspect of this type of experiment is to have a means by which to "visualize" whether a double stranded complex was formed, therefore identifying the piece of unknown DNA.

A schematic example of a DNA hybridization experiment is shown in Figure **1-2**. Here we see that a molecular "tag" is used to determine whether the DNA hybridization took place. This molecular tag is commonly a small organic molecule which, once excited with blue or UV light, fluoresces a signature color. These fluorescent tags are available in a range of colors and are attached to the unknown target DNA using well defined organic chemistry that places them in

positions that minimize the effect they have on the DNA hybridization [**1**]. The probe, or known DNA can be immobilized to a surface, also shown In Figure **1-2**. This enables one to spot or print many known DNA probe fragments on one surface so that the unknown, target DNA can be tested against many known samples on a single "chip". This type of high throughput analysis is commonly known as gene chip technology and is currently marketed by several companies including: Agilent Technologies, Bio-Rad, Perkin Elmer, Affymetrix, and many others.

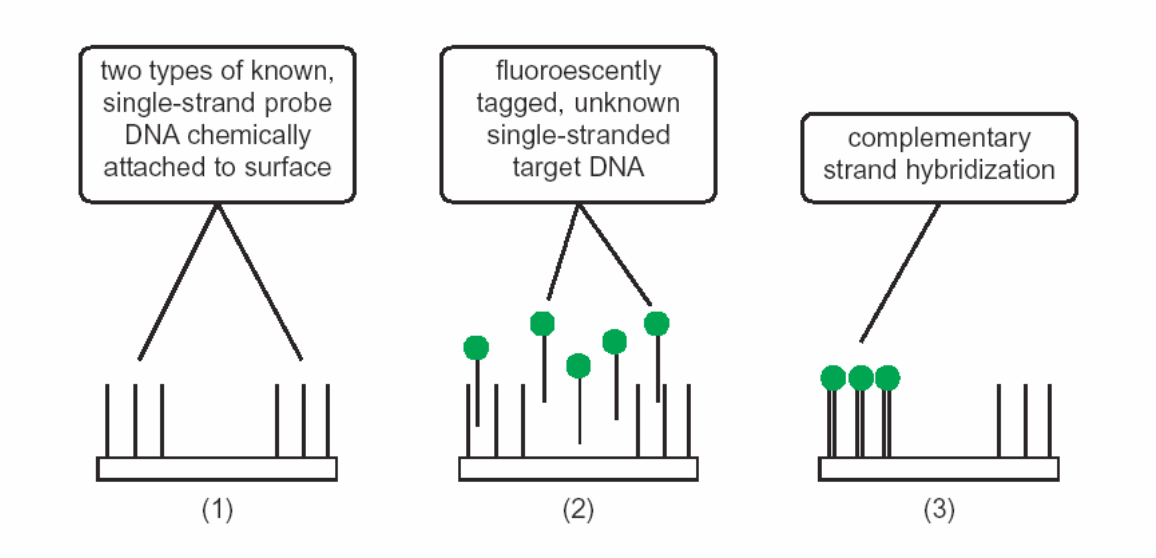

Figure **1-2**: A schematic of a DNA hybridization experiment showing the steps of: (1) spotting and attaching known single stranded probe DNA to a surface, (2) applying the unknown target DNA which is labeled with a fluorescent molecular tag, and (3) washing the surface to leave behind only the hybridized DNA, which can then be detected optically.

Gene chip systems are used primarily for research, but companies are developing and marketing them for use in clinical diagnosis. These systems typically include robotic printers, which print spots of DNA tens of microns wide,

and optical readers, which use lasers and high end confocal optics to read fluorescent images from the chips after the DNA hybridization reaction. Modern chips allow the screening of 10,000 DNA samples at once. This allows someone, for example, to print up to 10,000 variations of known skin cancer genes on the chip and then, with a patient's DNA, determine their exact skin cancer type. This type of analysis is very important for the treatment of cancers because current treatments include blind application of drugs in chemotherapy, which may or may not be effective on a given type of cancer. Unfortunately, the cost and complexity of a gene chip experiment is not yet attractive for clinical use. The chips themselves can cost thousands of dollars and the test equipment, printers and optical readers, cost in the hundreds of thousands of dollars range.

1.1.2 Protein Structure, Function and Analysis

The information contained within DNA essentially codes for the production of proteins. Proteins are also bio-polymers; however, they make use of twenty various building blocks (amino acids) contrary to DNA which has four. Not only is the sequence of a protein important to its function, but also its shape. The groups on each amino acid shape the protein through hydrogen bonding and interactions with the surrounding aqueous environment, and in most cases, protein shape is only stable in a given temperature, pH, and salinity range. Their shape is critical because of the "lock-and-key" type reactions that proteins

commonly perform [**2**]. In these lock and key reactions, proteins fit together in the reaction much like DNA fits together in complementary strand hybridization. Their shape and the exposed chemical groups allow proteins to form structural materials and catalyze reactions with each other and all other bio-molecules. Proteins create the structural fibers within cells, act as enzymes, transmit chemicals through the cell membranes, act as antibodies, act as the machinery that copies DNA, and even create the machinery that produces other proteins.

Knowing the sequence and shape of proteins found in the human body has obvious implications in medicine. Most pharmaceuticals work by interacting with proteins in some way. The human proteome project, similar to the genome project, has the goals of identifying every protein found in the human system and understanding its function [**2**]. This is a daunting task and may not be completed in our lifetime. One major hurdle is that protein structure is difficult to determine even if the sequence is known. The most reliable method for determining 3-D protein shape is x-ray crystallography; however, this technique is extremely difficult and not all proteins can be crystallized effectively. Quantum chemistry computer modeling is also used to determine shape, but computer power and algorithms are not fully capable as of yet, especially for large proteins. Another difficulty is that proteins are sometimes found in very small quantities (<10,000 molecules) within a cell and their concentrations differ wildly around the body and over time. Furthermore, proteins often have multiple functions that are regulated by a variety of input chemicals and proteins, making the pathways of their function highly complex.

In order to detect proteins and study their molecular interactions in a practical manner, experiments similar to DNA hybridization tests are performed. Fundamentally, one component of the reaction is tagged with a molecule that is easily detected. The placement of the tag on the molecule and how molecules are attached to surfaces are critical in these experiments. This concept is demonstrated for a protein-small molecule system in Figure **1-3**.

Other than using fluorescent molecules, protein study also makes use of other tagging systems. Catalytic proteins can be used as tags, and they cause color changes under certain conditions in what is called an Enzyme-linked immunosorbent assay (ELISA).[**2**] Gold nano-particles coated with proteins, which appear red in color, are also being used, with an example being home pregnancy tests [**3**]. More recently, semiconductor nano-particles with tailored fluorescent properties are being sold as tags by companies such as Quantum Dot Corporation. These semiconductor tags are currently very expensive but offer superior performance over organic fluorescent molecules, because they do not lose fluorescence efficiency over time [**4**].

In modern protein arrays, proteins are bound to a glass surface and tagged proteins (or other molecules) are allowed to interact, similar to a DNA gene chip. The analysis of these chips is nearly the same as a DNA chip, but they require more difficult handling because of the sensitivity of proteins to their environment and have complex chemical protocols [**5**].

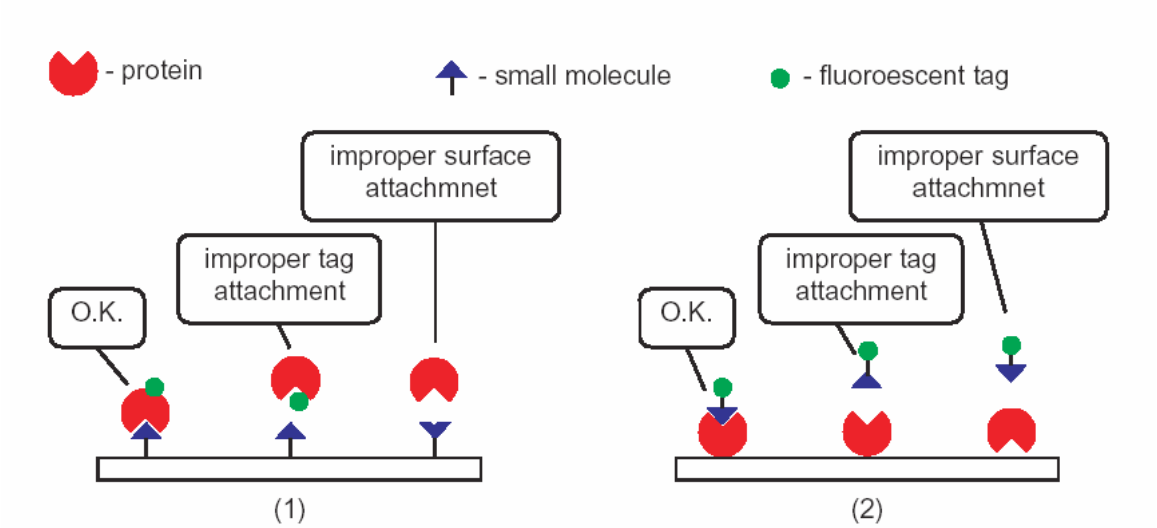

Figure **1-3**: Example of a protein-small molecule binding experiment where (1) the small molecule is bound to a surface and (2) where the protein is bound to a surface, demonstrating difficulties in tag and surface attachment.

1.2 Recent Approaches to Electrical Detection of Biochemical Interactions

All the previously discussed tagging approaches are based on optical detection. The expense of optical detection means and problems associated with fluorescent or other optical tags have driven research for alternatives. This has led to exploring electrical means for detecting bio-molecular species and their interactions. Electrical detection eliminates expensive optical systems and integrates easily with computer analysis systems. Electrical sensors also easily integrate into modern “lab-on-a-chip” and “micro total analysis” systems which are already commercialized. Often, research focuses on eliminating optical tags, which inherently interfere with the desired chemical interactions, or creating

electrically active tags which do not show transient effects such as photo-bleaching, a problem with molecular fluorophores. A variety of approaches to electrical sensing are reviewed below including: electrochemical analysis, surface capacitance measurements and field effect devices, electrical bridge sensors, and nano-gap sensors. The review will focus on the detection of biological molecules such as DNA and proteins because of their relevance to this thesis.

1.2.1 Electrochemical Sensors

Research has shown that electrochemical sensing in a variety of forms can be used to detect DNA [**6**][**7**][**8**]. DNA is a fairly robust molecule and therefore has been easier to study than proteins with electrochemistry. It has been known for many years that the adenine and guanine base pairs of DNA are susceptible to oxidation, but the exact reduction potentials in solution of the base pairs have been debated [**6**]. It has also proven difficult to detect guanidine by techniques such as cyclic voltammetry because of its high reduction potential [**6**]; however some groups have demonstrated the use of transition metal redox couples [**7**] and special types of AC voltammetry [**8**] to detect DNA and its base pairs.

One group [**9**] reported the use of an enzymatic protein tag (similar to ELISA) on DNA to detect hybridization through amperometric analysis. A schematic of their experiment is shown in Figure **1-4**. Here the target DNA is

tagged with a soybean peroxidase protein, which when brought in proximity to a special redox polymer electrode, creates a current through the catalytic reduction of H_2O_2. The probe DNA is chemically attached to the polymer electrodes, which allows the hybridization experiment to run with proper rinsing protocols. These workers calculated that this technique was able to detect as few as 40,000 peroxidase tags and therefore, 40,000 target strands of DNA on a 7um diameter electrode. Although the special, thermally stable peroxidase enabled proper hybridization reaction temperatures, it would be difficult to use this scheme in a commercial sensor because of the complexity of the protein-DNA tagging process and the relatively short lifetime of the peroxidase protein [**9**].

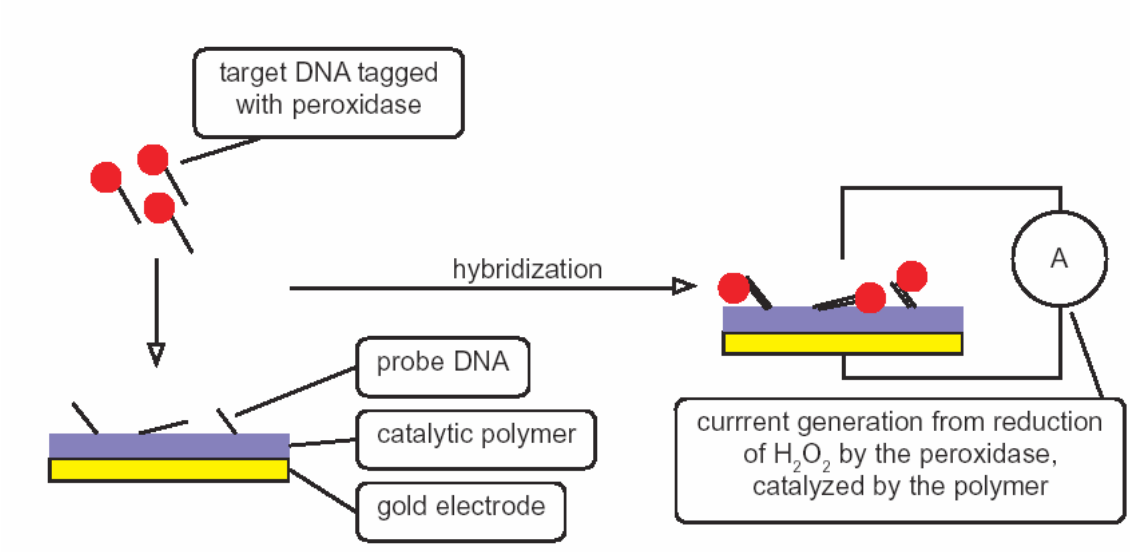

Figure **1-4**: Schematic of amperometric detection of hybridized DNA using a peroxidase tag.

Another group [**10**] recently reported a method of electrochemically detecting DNA hybridization by using two types of micro-spheres. A schematic of

their process is shown in Figure **1-5**. In their scheme, the probe DNA is attached to a magnetic bead. The target DNA is attached to a polystyrene bead impregnated with ferrocene, a common electrochemical reagent. After the hybridization reaction takes place, the magnetic beads are drawn to an electrode where chronopotentiometric, time dependant electrochemical detection, of the ferrocene takes place if the impregnated beads are present. They reported that this method enabled the detection of approximately 30,000 DNA molecules in a 50µl sample. One drawback of this technique is that the DNA hybridization times must be short in order to keep the ferrocene from diffusing out of the pre-loaded beads. This reduces the ability to selectivity hybridize the DNA.

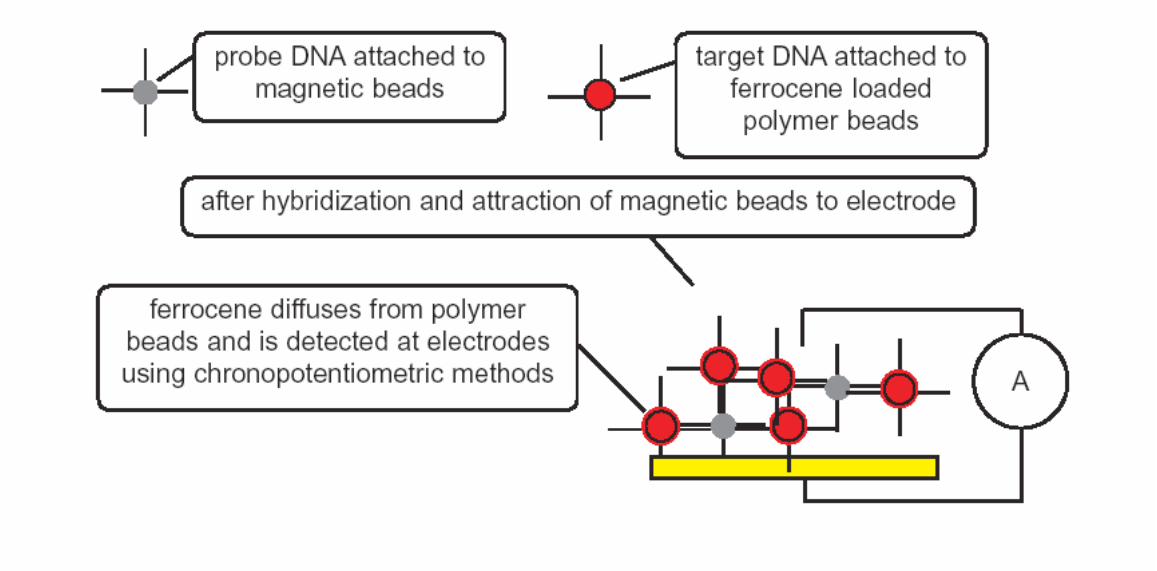

Figure **1-5**: Schematic showing the idea of using ferrocene impregnated beads as tags on the target DNA for electrical detection of a hybridization event.

1.2.2 Impedance and Field Effect Sensors

Researchers have studied the effect that DNA bound to an electrode surface has on the capacitance and, in general, the full impedance of electrochemical cells. Early studies by [**11**] used thiol-modified DNA attached to gold electrodes and capacitance monitoring to explore DNA assembly on the electrodes and subsequent hybridization. The results showed little if any changes in measured capacitance of the electrochemical cell and reported that the results were irreproducible from device to device. More recent work from [**12**] explored the use of a silicon electrode and high frequency impedance measurements to detect surface bound DNA. In this study, changes in impedance due to the hybridization of DNA on the surface of the electrode were shown. Using a circuit model these workers attributed the measured changes to impedance changes in the silicon electrode, not within the electrochemical double layer in the solution adjacent to the electrode. They attributed the changes in the silicon electrode properties to the proximity of the negatively charged DNA to the surface and the electrical potential changes in the silicon that it induced. Pushing this concept further, [**13**] used a field effect device with DNA attached to the gate oxide to exploit the negative charge that DNA can bring to a surface. They measured the impedance across the channel of the device at high frequencies to detect hybridization events. The DNA induced flat band voltage shifts in the device which were shown to be reversible upon the release (denaturization) of the non-surface bound strand of DNA. There was no mention

of the effect of salts in the solutions diffusing into and altering the gate oxide mobile charge, which may present a problem with this device.

1.2.3 Electrical Bridge Sensors

Two approaches have been explored using conductive bridge formation between electrodes to detect DNA hybridization events. One approach, schematically shown in Figure **1-6**, has been recently commercialized by Integrated Nano-Technologies LLC. [**14**]. Their technology uses lithographically defined microelectrodes on which they attach thiol-modified probe DNA. When a strand of DNA hybridizes to the probe DNA on both electrodes, spanning the gap, a series of chemical steps are used to grow silver onto the DNA bridge, electrically connecting the electrodes. The primary drawback of this technique is that long stretches of DNA (<500nm) must be used to span the gap because photolithography defines the electrodes. Because of this limitation, this sensor is marketed toward bio-warfare agent detection, in which long stretches of bacterial DNA need to be scanned.

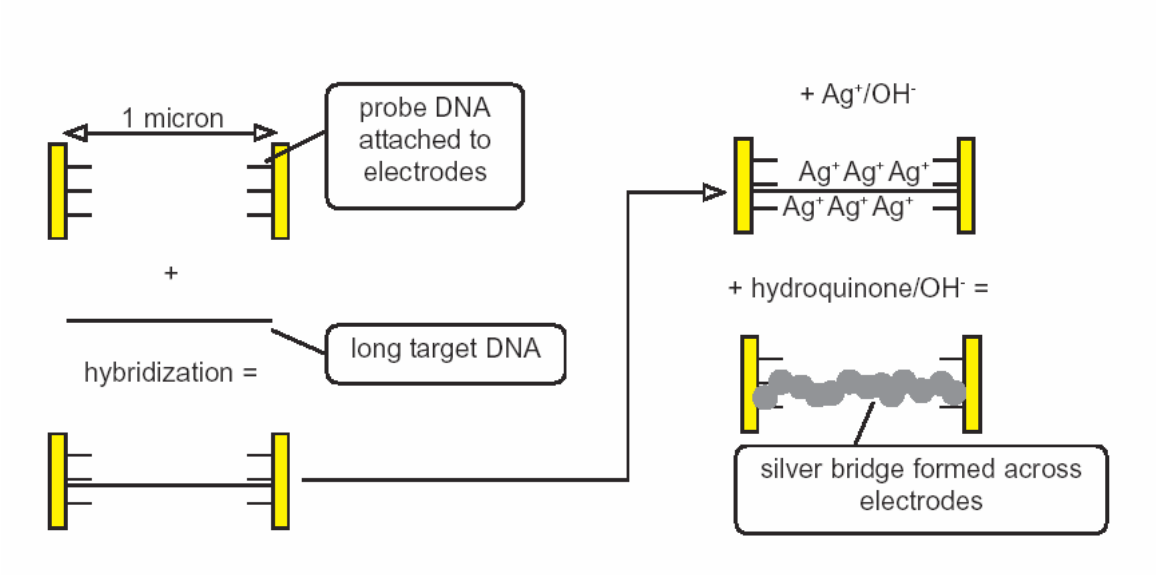

Figure **1-6**: Diagram showing steps in the detection of a stretch of DNA hybridized between two electrodes by growing a silver bridge on the DNA.

An approach similar to the above uses metal nanoparticles to enable the detection of hybridization of short strands of DNA, which makes the technique more versatile. This was first demonstrated in [**15**] and has been repeated in [**16**]. The general concept is shown in Figure **1-7**. Here the probe DNA is immobilized on a surface between the two electrodes, again defined by photolithography, and the target DNA is attached to gold nanoparticles. After a DNA hybridization event, silver is electrochemically plated onto the gold nanoparticles until a conductive bridge is formed. One surprising result of this study was that the nanoparticles aided in improving hybridization selectivity when varying salt concentrations in the wash. This was demonstrated with a single base pair mismatch system. Overall sensitivity of this type of sensor can be improved by decreasing the dimension of the electrode gap. However, even

electrodes with a small, 1μm separation require thousands of nanopaticles to bridge the gap, limiting its sensitivity. Furthermore, both this technique and the one previous rely on metal plating processes, which are sometimes difficult to reproducibly control [**17**].

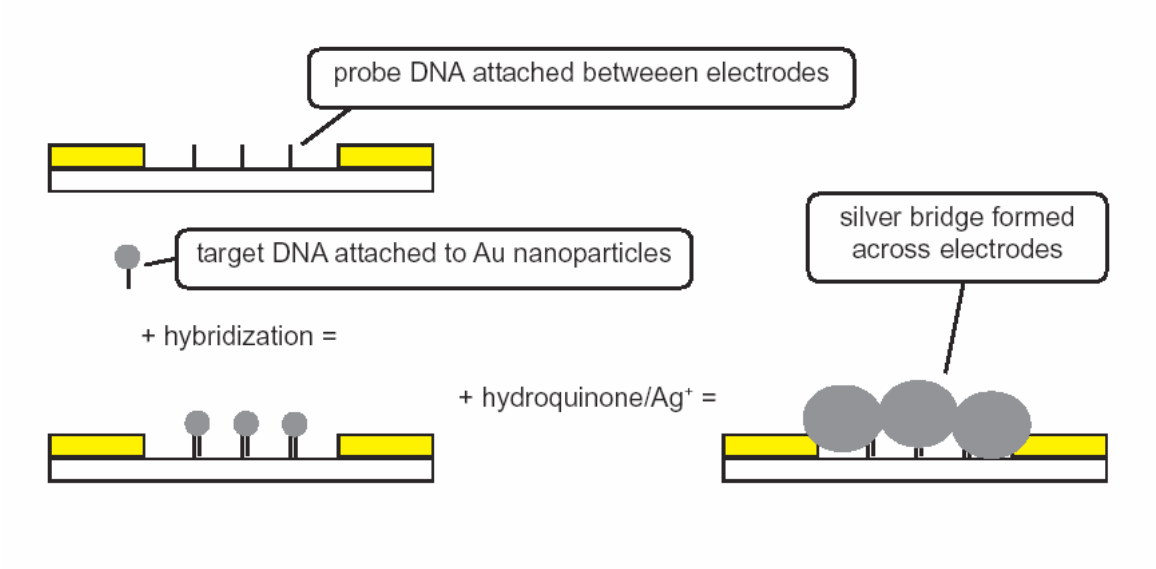

Figure **1-7**: Steps in the formation of a metal bridge between two electrodes using a nanoparticle tag system for detection of DNA hybridization.

1.2.4 Nano-Scale Gap Electrical Sensors

For the impedance and electrical bridge techniques presented above, there are obvious advantages to reducing the spacing between the device electrodes. For the impedance measurements, reducing the spacing between the working and counter electrodes (if there is such a distinction in the setup) allows for the reduction of series impedance due to the solution and increases the contribution of the electrode surface conditions to the measured impedance.

For the electrical bridge techniques, a small gap enables shorter strands of DNA to be detected using the direct plating technique and increases the sensitivity of the nanoparticle technique by reducing the number of beads required to span the gap. Because of these reasons, and a drive from the molecular electronics community, groups have been studying low cost (non e-beam lithography) methods of producing capacitor-like structures with nano-scale electrode separations. Most of these methods suffer from extreme irreproducibility issues and structures that are not ideal, with planar open electrodes instead of a parallel plate capacitor configuration [**18**], [**19**].

Our group recently reported a cost-effective method for producing a nanometer scale gap electrode structure [**20**]. This novel fabrication method uses a sacrificial layer and standard photolithography processes to produce the structure shown in Figure **1-8**. In the reported work, self-assembly of alkanethiols and DNA on gold electrodes was studied by impedance changes in the device, taking advantage of its unique structure. Preliminary work was also presented in using a nanoparticle system within the gap. Here, the presence of nanoparticles, labeled with proteins, caused the device to collapse and electrically short at relatively low voltages. There were difficulties in implementing the technique on a full bio-molecular interaction study, because the materials chosen for the electrodes either provided chemically active electrodes (gold) with poor voltage stability or high voltage stability (platinum electrodes) with no chemical activity, both of which are required for the nanoparticle technique to work effectively. Furthermore, the chemistry used to perform

chemical attachment to the electrodes and effective hybridization washing protocols were not explored thoroughly because of the work's emphasis on fabrication. This novel and fundamental preliminary work is the foundation of the work presented in this thesis. The goal here in the new work is to improve the device design, fabrication and chemistry and to further explore the possibility of this technology's becoming a practical commercial concept.

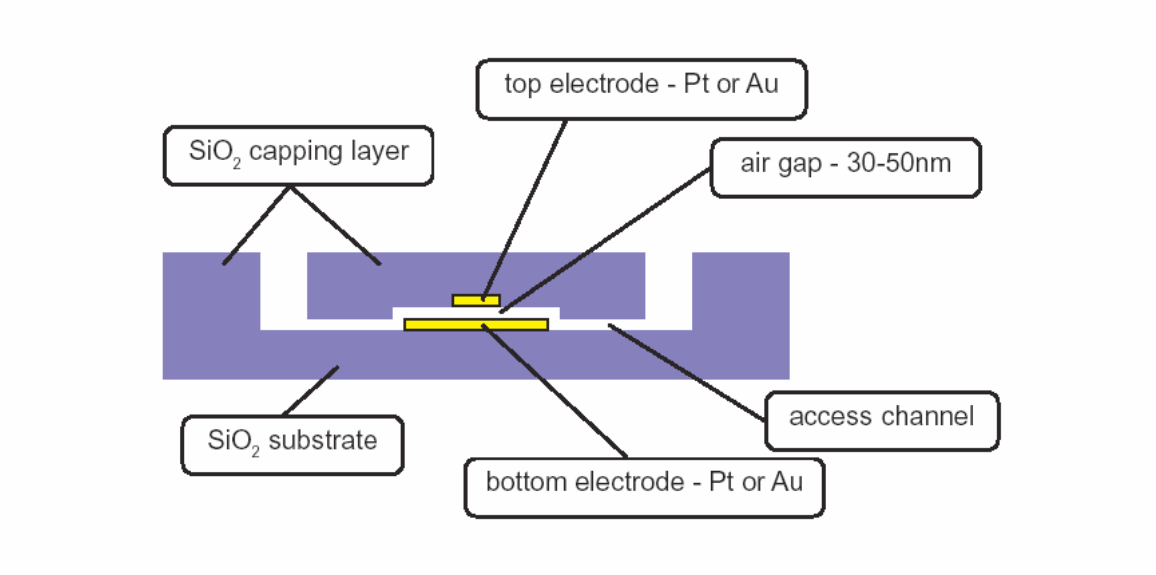

Figure **1-8**: Diagram of a nano-scale gap electrode structure produced using a novel sacrificial layer technology and standard photolithography.

1.3 Proposed Approach and Project Goals

The overall goal of this research is to improve the nano-gap sensor concept and the electrical detection scheme for bio-molecular interactions. The intention is to significantly advance the work demonstrated previously by our group in detecting bio-molecular interactions using molecular self-assembly

within a nano-scale gap electrode device. To achieve this, three specific goals of this work are as follows:

1. Fabricate a device which combines the high voltage stability of our group's previously fabricated platinum electrode devices with the ability to run sulfur based surface chemistry on the electrodes as in our group's previously fabricated gold electrode devices

2. Develop improved self-assembling electrode surface chemistries and a biological interaction test system to monitor and evaluate a bio-molecular reaction within the device

3. Use the improved device and chemistry to demonstrate electrical bio-molecular interaction detection

In order to achieve goal number one, various electrode compositions and sacrificial layer materials will be explored. For goal number two, a polyethylene glycol (PEG) self-assembling chemistry with a small molecule (biotin) terminus will be developed which will bind with the protein streptavidin and thereby with streptavidin coated nanoparticles. Combining these two and refining a "breakdown" electrical detection technique will be the approach to goal number three. All these approaches will be "firsts." The rationale behind the details of the approaches taken will be presented in the methods section of this document prior to presenting and discussing experimental results.

Achieving these goals will demonstrate unique detection schemes enabled by a novel device structure. Furthermore, the use of our device over other gap structures, combining a nano-gap structure and the ability to chemically functionalize the electrodes, will improve many of the detection schemes reviewed in Section **1.2**. This is important from a commercial point of view, because a device that enables a variety of detection schemes is a lower risk platform to develop than a specialized one. The realization of these goals will be evaluated in the conclusions section of this document, and comments as to the commercial viability of this work will be presented.

1.4 References

1. Agilent Technologies, "Agilent Fluorescent Direct Label Kit," [online document], June 2003, version 2.1, Available HTTP: //www.chem.agilent.com/temp/rad9741F/.

2. B. Albert, A. Johnson, J. Lewis, M. Raff, K. Roberts and P. Walker, Molecular Biology of the Cell, 4th ed.,New York, NY: Garland Science, 2002.

3. J. Burstein, G. Braunstein, "Urine pregnancy tests from antiquity to the present," Early Pregnancy: Biology and Medicine 1, pp. 288-296, 1995.

4. S. Jaiswal, "Long-term multiple color imaging of live cells using quantum dot conjugates," Nature Biotechnology, vol. 12, pp. 47-51, 2003.

5. G. MacBeath and S. Schreiber, "Printing Proteins for High-Throughput Function Determination," Science, vol. 289, pp. 1760-1763, 2000.

6. S. Steenken and S. Jovanovic, "How Easily Oxidizable is DNA? One-Electron Reduction Potentials of Adenosine and Guanosine Radicals in Aqueous Solution," Journal of the American Chemical Society, vol. 119, pp. 617-618, 1997.

7. M. E. Napier, C. R. Loomis, M. F. Sistare, J. Kim, A. E. Eckhardt, and H. H. Thorp, "Probing Biomolecule Recognition with Electron Transfer: Electrochemical Sensors for DNA Hybridization," Boiconjugate Chemistry, vol. 8, pp. 906-913, 1997.

8. P. Singhal and W. Kuhr, "Ultrasensitive Voltammetric Detection of Underivatized Oligonucleotides and DNA," Analytical Chemistry, vol. 69, pp. 4828-4832, 1997.

9. D. J. Caruana and A. Heller, "Enzyme-Amplified Amperometric Detection of Hybridization and of Single Base Pair Mutation in an 18-Base Oligonucleotide on a 7-um-Diameter Microelectrode," Journal of the Americal Chemical Society, vol. 121, pp. 769-774, 1999.

10. J. Wang, R. Polsky, A. Merkoci, and K. L. Turner, ""Electroactive Beads" for Ultrasensitive DNA Detection," Langmuir, vol. 19(4), pp.989-991, 2003.

11. C. Berggren, P. Stalhandske, J. Brundell, and G. Johansson, "A Feasibility Study of a Capacitive Biosensor for Direct Detection of DNA Hybridization," Electroanalysis, vol. 11(3), pp. 156-160, 1999.

12. W. Cai, J. Peck, D. W. van der Weide, and R. Hamers, "Direct Electrical Detection of Hybridization at DNA-modified Silicon Surfaces," Biosensors and Bioelectronics, vol. x, xx-xx, xxxx.

13. E. Souteyrand, J. P. Cloarec, J. R. Martin, C. Wilson, I. Lawrence, S. Mikkelsen, and M. F. Lawrence, "Direct Detection of the Hybridization of Synthetic Homo-Oligomer DNA Sequences by Field Effect," Journal of Physical Chemistry B, vol. 101, pp. 2980-2985, 1997.

14. E. Braun, Y. Eichen, U. Sivan, and G. Ben-Yoseph, "DNA-Templated Assembly and Electrode Attachment of a Conducting Silver Wire," Nature, vol. 391, pp. 775-778, 1998.

15. S. Park, T. A. Taton, and C. A. Mirkin, "Array-Based Electrical Detection of DNA with Nanoparticle Probes," Science, vol. 295, pp. 1503-1506, 2002.

16. M. Xue, J. Li, W. Xu, Z. Lu, K. L. Wang, P. K. Po, and M. Chang, "A Self-Assembly Conductive Device for Direct DNA Identification in Integrated Microarray Based System," in Electron Devices Meeting, 2002, IEDM '02. Digest. International, 2002, pp. 207-210.

17. Y. Okinaka and M. Hoshino, "Some Recent Topics in Gold Plating for Electronics Applications," Gold Bulletin, vol. 31(1), pp. 3-13, 1998.

18. G. Philipp, T. Weimann, P. Hinze, M. Burghard, and J. Weis, "Shadow Evaporation Method for Fabrication of sub 10nm Gaps Between Metal Electrodes," Microelectronic Engineering, vol. 46, pp. 157-160, 1999.

19. H. Park, A. K. L. Lim, and P. Alivisatos, "Fabrication of Metallic Electrodes with Nanometer Separation by Electromigration," Applied Physics Letters, vol. 75(2), pp. 301-303, 1999.

20. W. J. Nam, "Molecular Scale Gap Sensors Fabricated Using Sacrificial Layers and Self-Assembly," dissertation, University Park: Penn State University, 2003.

Chapter 2

Experimental Methods

The fabrication, chemical modification, and electrical characterization methods used for this work are given below in detail. The structure and fabrication of the nano-gap device is unique; however, standard micro-machining processes and photolithography are used in the given process flow. Chemically modifying the device electrodes makes the use of self-assembling thiol-based chemistry, and a novel scheme is presented to link the biological molecule biotin to their surface. The devices are characterized electrically to monitor these reactions and the methods for this will be shown as well.

2.1 Device Fabrication

Fabrication of the nano-gap device was performed at the Penn State Nanofabrication Facility. The cleanroom environment of this facility reduces the number of particulate related defects, which is especially important for devices with nano-scale features. The process flow uses four photolithography mask steps, a variety of material deposition steps, and a sacrificial layer removal to create the nano-gap structure. The fabrication process begins with the preparation of an insulating substrate (wafer) and ends with sacrificial layer removal and device encapsulation. The device is constructed using thin-films

deposited on the substrate in what is commonly referred to a surface micro-machining.

There were several variations of materials chosen for the device electrodes and sacrificial layers. Observations from prior work [**1**] and results obtained during this project guided the selection of trial materials, which is done in consideration of fabrication complexity and cost. The goal of device fabrication was to fabricate a device with high strength and chemically active electrodes to thiol-based chemistry, combing the properties of the previously fabricated platinum electrode (strength) and gold electrode (functionality) devices. Several approaches were explored, with varying results given in Chapter 3.

2.1.1 Substrate Preparation

Two substrate materials were used to fabricate the nano-gap devices: quartz and low-sodium aluminosilicate glass (Corning 1737™). These materials were chosen because of their compatibility in the fabrication facility equipment (low salt content), their insulating properties, and their low surface roughness. Both substrates had dimensions of a 100mm diameter wafer with 1mm thickness. The quarts wafers are more expensive than the aluminosilicate glass but have better insulating properties because of the high purity of quartz.

The substrates were prepared for fabrication with a chemical clean. The wafers were washed in a bath of NanoStrip™ (Cyantek Inc.) on a 70^{o}C hotplate for 5min to remove organic contaminates such as oil and grease. After a

thorough rinse with de-ionized water (DI water), the substrates were inspected for defects and particulates. The substrates were used within a couple days of preparation to avoid contamination.

2.1.2 Bottom Electrode Patterning and Deposition

The first mask step defines the bottom electrode of the nano-gap and both electrode contact pads. Here, a lift-off process is used to pattern the metal on the substrate after metal deposition. The lift-off process used for this work, shown schematically in Figure **2-1**, makes the use of a bi-layer photoresist. This two-layer resist forms an undercut as shown in the figure, which aides the lift-off process and produces a metal pattern with uniform thickness and clean edges.

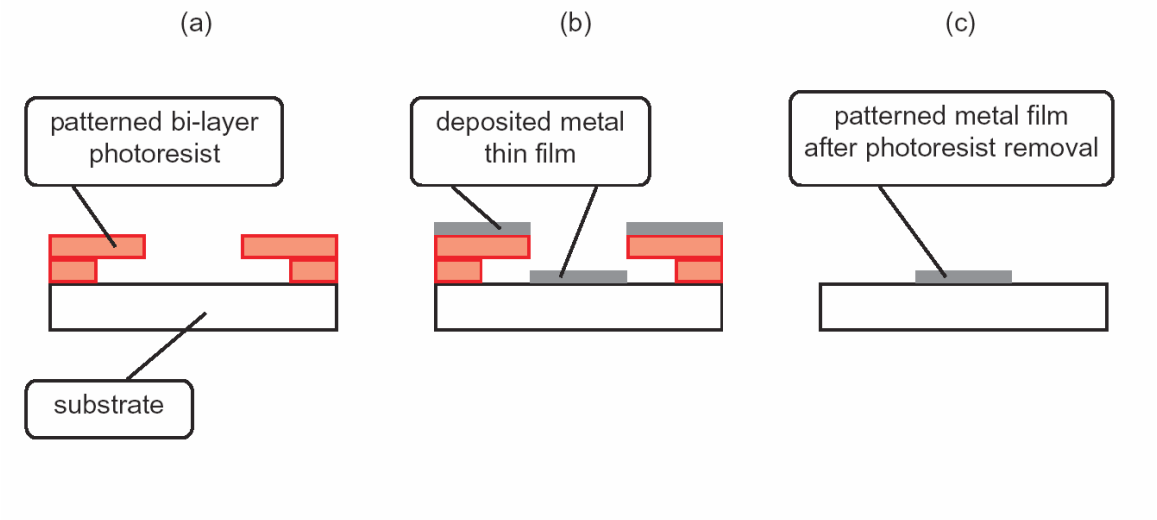

Figure **2-1**: Schematic of a metal lift-off process showing the steps of a) creating the pattern in a bi-layer photoresist, b) depositing a metal film, and c) removing the photoresist.

The processing parameters for the bi-layer photoresist process are given in Table **2-1**. If processed correctly, the undercut can be visualized with optical microscopy as shown in Figure **2-2**.

Table **2-1**: Processing parameters for bi-layer lift-off photoresist

1st Photoresist – LOR 5A (Shipley Inc.)	
Application	Dynamic application @ 500RPM, 30sec
Spin-coat	4000RPM, 50sec
Soft-bake	6min, 184°C hotplate
2nd Photoresist – SPR 3012 (Shipley Inc.)	
Application	Dynamic application @ 500RPM, 10sec
Spin-coat	4000RPM, 50sec
Soft-bake	90sec, 115°C hotplate
UV Exposure – Karl Suss MA6 Contact Aligner	
Exposure	4.2sec @ 12mW
Post-exposure bake	90sec, 115°C hotplate
Developer – CD-26 (Shipley Inc.)	4-6min, room temperature
DI water rinse	5min

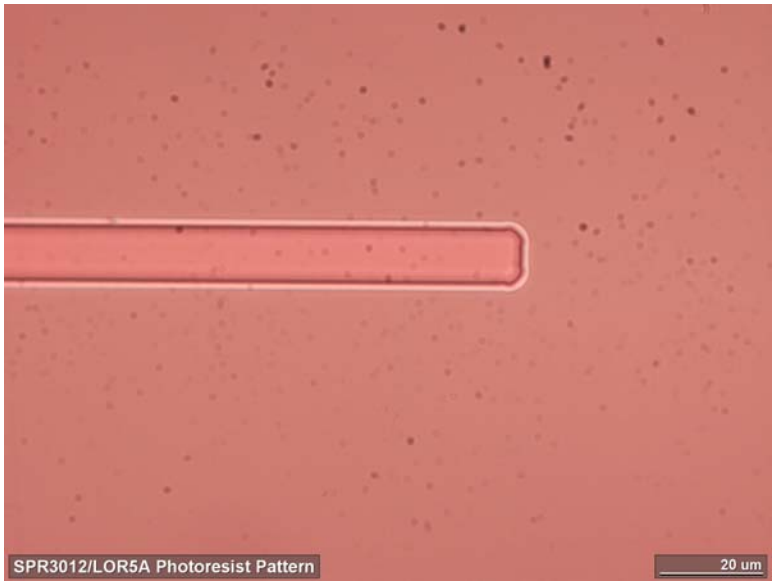

Figure **2-2**: Picture of bi-layer photoresist showing the undercut as a pale halo surrounding the pattern.

Three types of bottom electrode metal configurations were explored: Pt with Ti adhesion layer, Au with Cr adhesion layer, and Au graded with Ti. All films were deposited in a vacuum evaporator system (Kurt Lesker Inc.) with e-beam and thermal source capability. Evaporator conditions for each of the electrode types are given in Table **2-2**, Table **2-4**, and Table **2-3**. The target thickness of 30nm was achieved through proper calibration of the crystal thickness monitor and confirmed with atomic force microscopy AFM (Digital Instruments Inc.). All metals used in these and subsequent steps were obtained from Alfa Aesar Inc. and were a minimum of 99.999% pure.

Table **2-2**: Evaporation process parameters for Pt bottom electrode with Ti adhesion layer

Base Pressure	< $5x10^{-6}$ torr
Ti evaporation – e-gun	5nm @ .05nm/sec
Cool after Ti evaporation	3min
Pt evaporation – e-gun	25nm @ .05nm/sec
Cool prior to system vent	15min
Final film thickness	30nm

Table **2-3**: Evaporation process parameters for Au bottom electrode with Cr adhesion layer

Base Pressure	< $5x10^{-6}$ torr
Cr evaporation – e-gun	5nm @ .05nm/sec
Cool after Cr evaporation	None
Au evaporation – thermal, W boat	25nm @ .05nm/sec
Cool prior to system vent	15min
Final film thickness	30nm

Table **2-4**: Evaporation process parameters for Au graded with Ti bottom electrode

Base Pressure	< $5x10^{-6}$ torr
Au – thermal, Ti – e-gun simultaneously	Crystal thickness monitor on Au settings
Begin Ti evaporation @ .01nm/sec	Deposit 1nm
Ramp Au to .02nm/sec	Up to 3nm
Ramp Au to .03nm/sec	Up to 5nm
Lower Ti to .02nm/sec	Up to 7nm
Ramp Au to .04nm/sec	Up to 10nm
Turn off Ti	Up to 11nm
Ramp Au to .05nm/sec	Up to 19nm
Cool prior to system vent	15min
Final Thickness	30nm

The lift-off process was completed by removing the photoresist in 1165 Photoresist Remover (Shipley Inc.) at 70^{o}C. The removal time of the photoresist varied with the different metal films because of their varying rigidity. The brittle platinum films cracked on the photoresist, allowing the removal of the resist in 5min. The ductile gold films protected the photoresist well against the remover causing removal times of 25min. After the photoresist was completely removed, the wafer was rinsed aggressively with DI water for 5min and blown dry with nitrogen. A schematic of the device after completion of this step is given in Figure **2-3**.

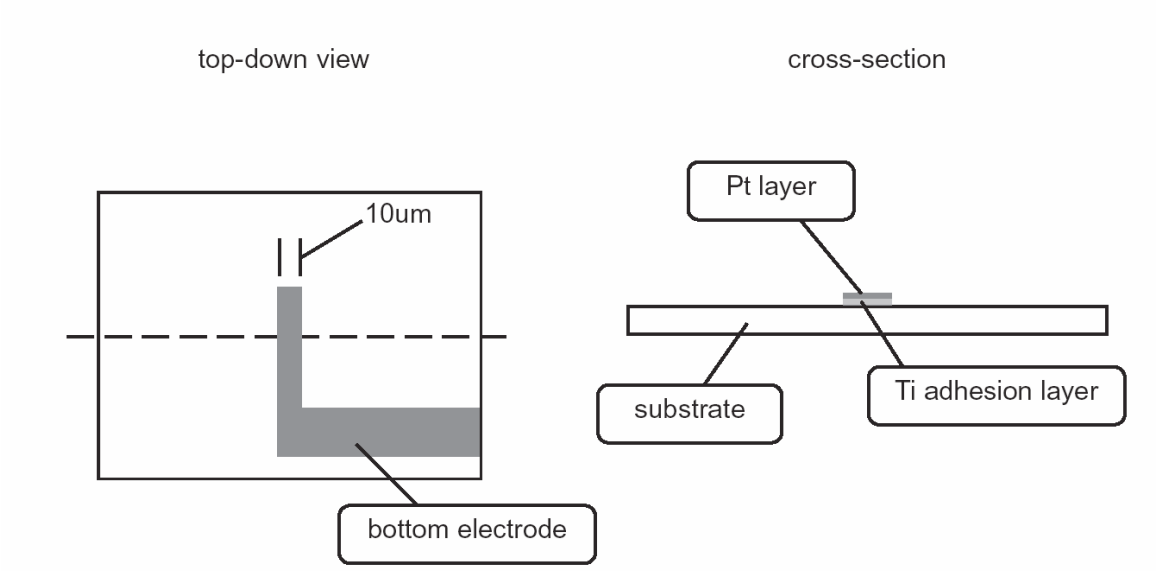

Figure **2-3**: Schematic of a nano-gap device after the bottom electrode lift-off step. A device with a Pt electrode is shown.

2.1.3 Sacrificial Layer Patterning and Deposition

Two metals, nickel and copper, were explored as the sacrificial layer in the nano-gap device. These metals were chosen because of their fast etch rates and excellent etch selectivity over the device electrodes. The second mask step defines the sacrificial layer region with another lift-off process, using the same photolithography process in Table 2-1. Evaporator conditions for the sacrificial layer depositions, performed in the same evaporation system as the electrodes, are given in Table **2-5** and Table **2-6**. A thickness of 50nm for the sacrificial layer is used in this work. This thickness can be varied and defines the final electrode gap spacing of the device. The ability to control the gap spacing by simply changing the sacrificial layer thickness is one of the major advantages of our

technique in creating nano-gap structures. The lift-off procedure is completed in the same manner as described in the previous section, and a schematic of the device after this step is given in Figure **2-4**.

Table **2-5**: Evaporation process parameters for Ni sacrificial layer

Base Pressure	< $5x10^{-6}$ torr
Ni evaporation – e-gun	50nm @ .05nm/sec
Cool prior to system vent	15min
Final film thickness	50nm

Table **2-6**: Evaporation process parameters for Cu sacrificial layer

Base Pressure	< $5x10^{-6}$ torr
Cu evaporation – thermal	50nm @ .05nm/sec
Cool prior to system vent	15min
Final film thickness	50nm

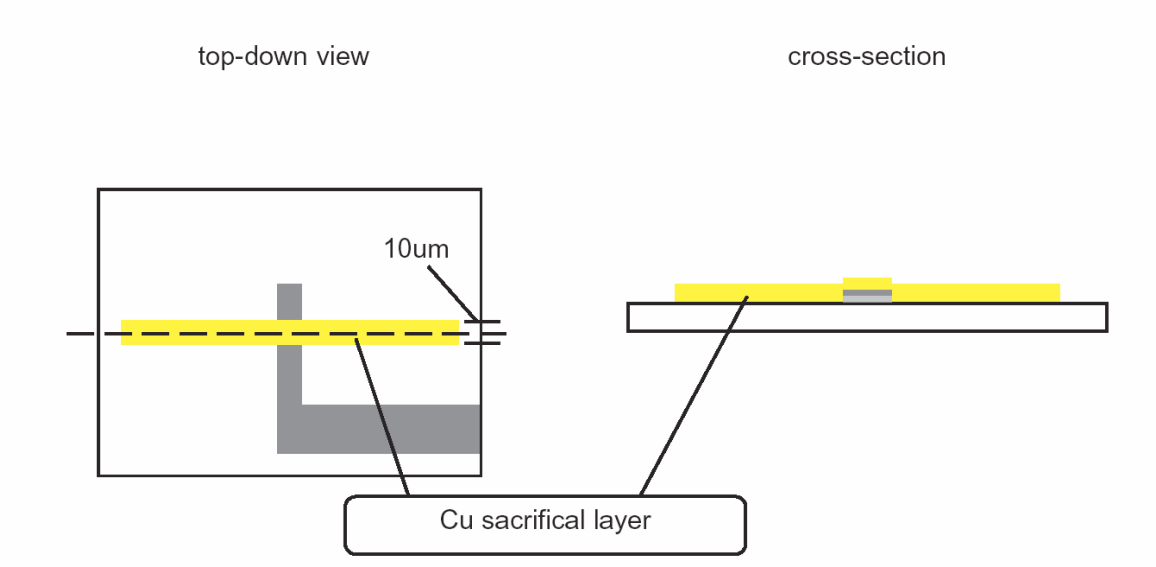

Figure **2-4**: Schematic of a nano-gap device after the sacrificial layer lift-off step.

2.1.4 Top Electrode Patterning and Deposition

Four types of top electrode metal configurations were explored: Pt with Ti adhesion layer, Au with Cr adhesion layer, and Au graded with Ti, and Au graded with Pt with Ti adhesion layer. The third mask and another lift-off process were used to pattern the material. For the bi-layer films (Pt-Ti, Au-Cr), the evaporation processes were similar to those in Table 2-2 and Table 2-3 except that the Pt and Au films were deposited first. The graded Au-Ti film was deposited in reverse order than that shown in Table 2-4. The parameters for the graded Au-Pt film with Ti adhesion layer are given in Table **2-7**. A schematic of the device following top electrode deposition is given in Figure **2-5**.

Table **2-7**: Evaporation process parameters for the Au graded with Pt top electrode with Ti adhesion layer

Base Pressure	< $5x10^{-6}$ torr
Au – thermal, Pt – e-gun simultaneously	Crystal thickness monitor on Au settings
Begin Au evaporation @ .01nm/sec	Deposit 5nm
Ramp Pt to .02nm/sec	Up to 10nm
Ramp Pt to .03nm/sec	Up to 15nm
Ramp Pt to .04nm/sec	Up to 20nm
Turn off Au	Up to 25nm
Cool prior to Ti evaporation	3min
Ti evaporation – e-gun	5nm @ .05nm/sec
Cool prior to system vent	15min
Final film thickness	30nm

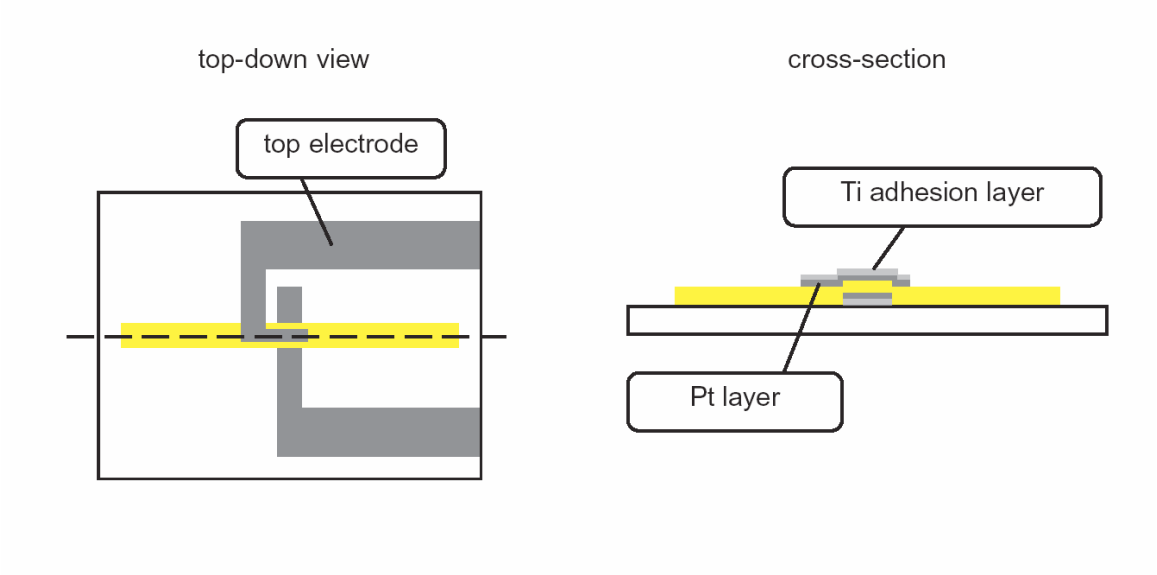

Figure **2-5**: Schematic of a nano-gap device after the top electrode lift-off step. A device with a Pt electrode is shown.

2.1.5 Capping Layer Deposition

The capping layer insulates the electrodes from the electrolytic solution during device operation and provides mechanical support for the top electrode to prevent mechanical collapse. In this work, a low-temperature deposited silicon dioxide served as the capping layer. Low-temperature (<300^{o}C) deposition of the silicon dioxide is necessary to prevent metallic migration and significant expansion of the metals, which may cause device performance loss. An electron cyclotron resonance plasma enhanced chemical vapor deposition (ECR-PECVD) machine (Plasma Therm Inc.) deposited the capping layer film in a vacuum environment. This machine creates high density plasma, which excites numerous chemically active species within the plasma at low gas temperatures

(< 100^{o}C). These active species grow films on surfaces as determined by the gas chemistry, silane and oxygen in this case.

Prior to use, the ECR-PECVD system was cleaned with IPA and DI water to remove prior deposited films on the surface of the chamber. Then hydrogen and oxygen plasmas were used to remove water and organic contaminants. Prior to loading the device substrates, a 150nm thick silicon dioxide film was deposited to coat the chamber walls.

Surface preparation of the devices prior to capping layer deposition is important because the adhesion between the silicon dioxide and the top electrode is critical for device performance. A dehydration bake was used to remove surface water prior to loading the substrate into the ECR-PECVD vacuum system. Ni sacrificial layer devices were dehydration baked for 15 min on a 150^{o}C hotplate, and Cu sacrificial layer devices were baked for 15 min on a 100^{o}C hotplate. The Cu films oxidized severely at higher hotplate temperatures. Once in the vacuum system, the surface was further conditioned by running a 3min oxygen plasma to remove trace organic contaminants and to created an oxygen rich surface on the adhesion metal (Cr or Ti) for good adhesion to the silicon dioxide. The process parameters for the surface conditioning oxygen plasma are given in Table **2-8**.

Table **2-8**: Process parameters for oxygen plasma surface treatment

Base pressure	< $5x10^{-7}$ torr
Process pressure	2.5mtorr
O_2 gas flow rate	19sccm
Ar gar flow rate	3sccm
Substrate temperature	100^oC
Microwave power	900W
Time	3min

The capping layer is deposited in 1um increments until the desired thickness is obtained. After each 1um deposition the system is allowed to cool and the substrate is rotated 90^o to ensure thickness uniformity. A mixture of silane and oxygen with an argon stabilizer was used to grow the silicon dioxide films. The machine parameters for each 1um deposition are given in Table **2-9**. Typically a 10um capping layer was used, but a 4um capping layer device was also produced. The quality and deposition rate of the oxide was checked by ellipsometery (Gaertner Inc.) prior to capping layer deposition. A schematic and picture of a device following capping layer deposition is given in Figure **2-6**.

Table **2-9**: Process parameters for 1um silicon dioxide capping layer deposition

Base pressure	< $5x10^{-7}$ torr
Process pressure	4mtorr
O_2 gas flow rate	5.1sccm
Ar gar flow rate	3sccm
SiH_4 gas flow rate	4sccm
Substrate temperature	100^oC
Microwave power	900W
Time	75min

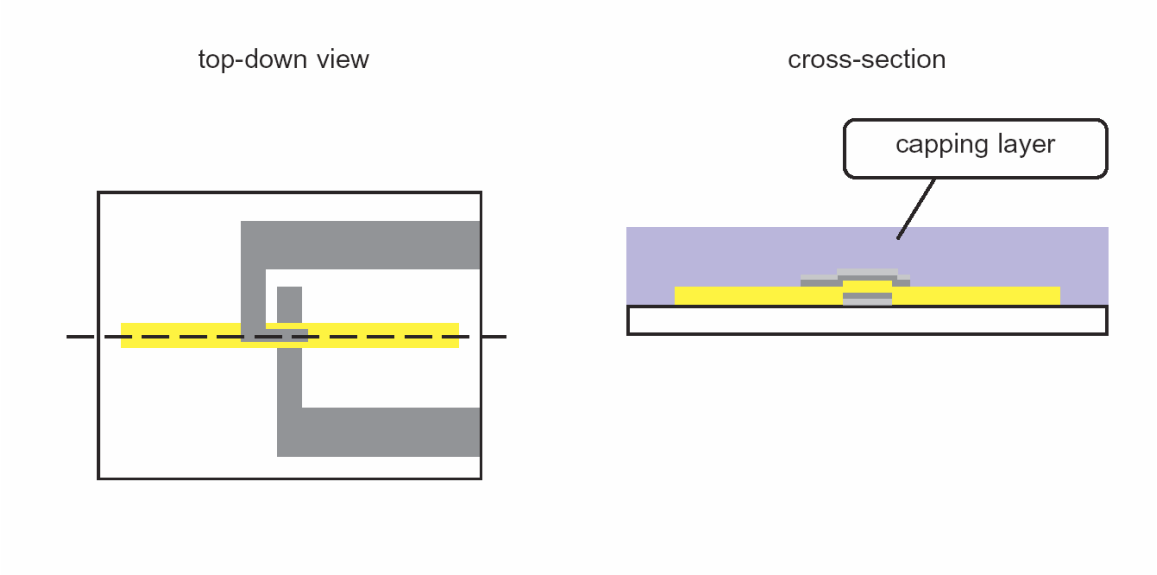

Figure **2-6**: Schematic of a nano-gap device after the silicon dioxide capping layer deposition.

2.1.6 Access Hole Definition and Etching

Access holes are crated through the capping layer to allow etchants to remove the sacrificial layer and to allow chemical transport into the nano-gap during device use. Photoresist (Shipley 1813^{TM}) was used as the etch mask and was patterned using the fourth photolithography mask. The parameters for this photoresist process are given in Table **2-10**. The silicon dioxide was etched with a 10% HF dilution in DI water for 45 seconds to form the access holes. After a thorough DI water rinse, the photoresist was removed with acetone and isopropyl alcohol (IPA). The wet etch of silicon dioxide in HF is isotropic, so the access holes undercut the photoresist pattern by approximately 10um. This limits the ultimate proximity of the access holes on either end of the nano-channel. An

etch study with longer etch times was also performed to determine the effects of lover etching the access holes. A schematic a device following this step is given in Figure **2-7**.

Table **2-10**: Process parameters for access hole definition photoresist step

Photoresist – 1813 (Shipley Inc.)	
Application	Dynamic application @ 500RPM, 10sec
Spin-coat	4000RPM, 50sec
Soft-bake	90sec, 115°C hotplate
UV Exposure – Karl Suss MA6 Contact Aligner	
Exposure	4.5sec @ 12mW
Developer – CD-26 (Shipley Inc.)	45sec, room temperature
DI water rinse	5min

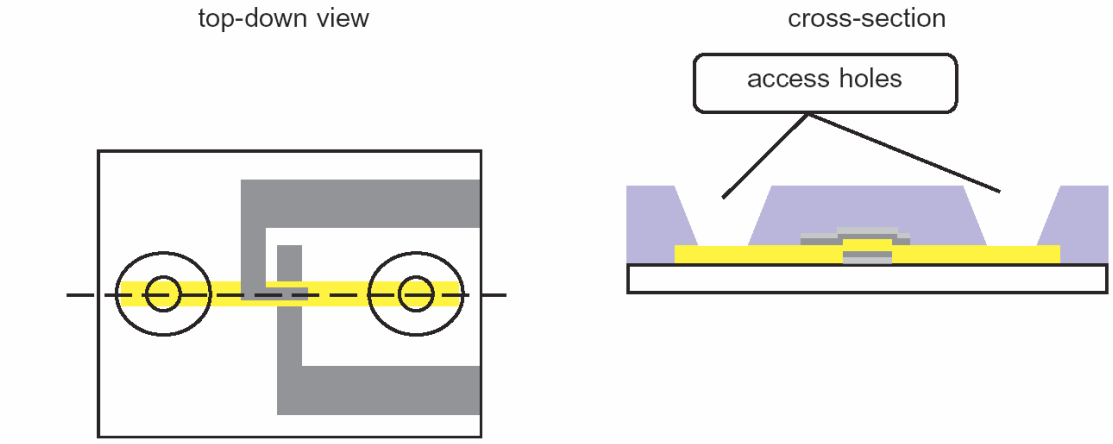

Figure **2-7**: Schematic of a nano-gap device after the etching of access holes in the capping layer.

2.1.7 Sacrificial Layer Etching

The final step in device fabrication is the etching of the sacrificial layer to form the nano-gap electrode structure. Two liquid etchants were used to remove the Cu and Ni sacrificial layers, hydrochloric acid based Nickel etch Type I (Transene Inc.) and nitric acid based Nickel etch Type TFB (Transene Inc.). A 20 min etch in a 70^{o}C solution of either type of etchant for either type of sacrificial layer ensured complete sacrificial layer removal. After etching, the device was rinsed for 20 min in DI water to remove the residual etchants, which must diffuse out of the nano-channel. After sacrificial layer removal, the device structure is as shown in Figure **2-8**.

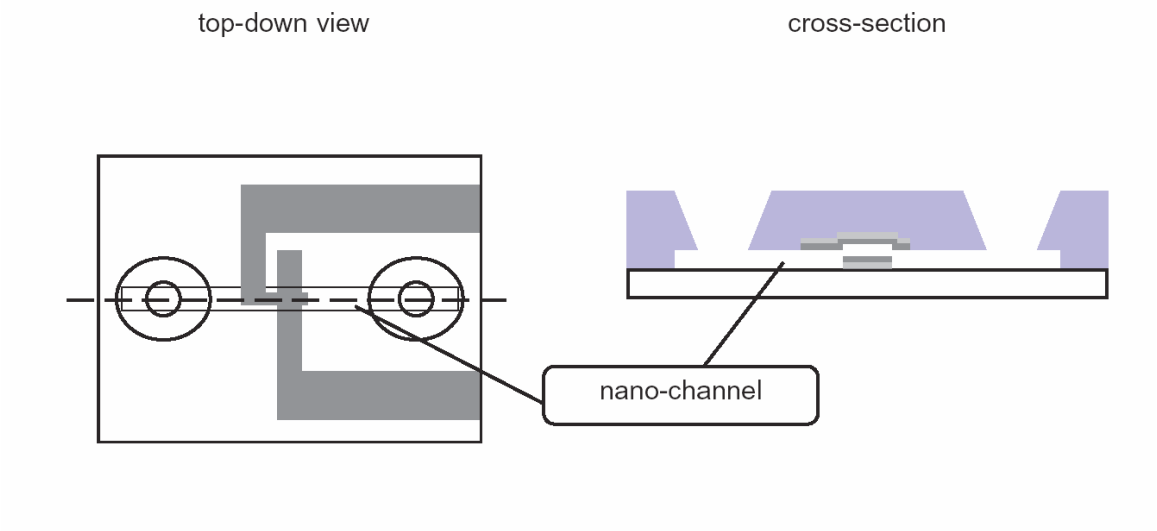

Figure **2-8**: Schematic of a nano-gap device after the etching of the sacrificial layer.

2.1.8 Device Encapsulation

Device encapsulation is important for this device, because liquid and electrical contacts must be made. The electrical contacts for each device are insulated until the edge of each chip where contact pads for micro-probes are located. This is shown in Figure **2-9**. The liquid must be in contact with the access holes and nano-channels at he center of the chip. To keep the liquid contained, polypropylene wells were adhered to the chip also as shown in Figure 2-9.

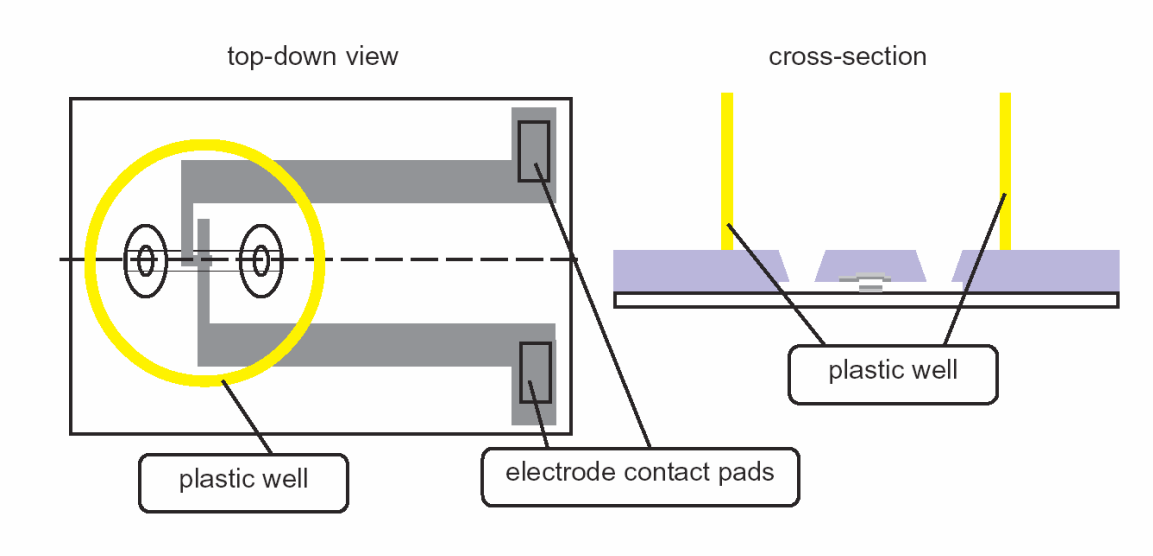

Figure **2-9**: Schematic of an encapsulated device, showing a plastic well adhered to the chip to separate the liquid which fills the nano-gap from the exposed contact pads.

2.2 Surface Modifications and Bio-chemistry

A fundamental aspect of the nano-gap device as a bio-chemical detector is the ability to modify the electrodes with organic species. This work makes use of sulfur based surface chemistry to link organic species to the inorganic Pt or Au electrode surfaces. The ultimate goal is to attach biological species to the electrode surfaces through organic linking chemistries. This section presents the novel linking chemistry used to attach biotin to the nano-gap electrodes and the experimental procedures for determining chemical attachment ability (functionality) on the electrodes.

2.2.1 Thiol-based Surface Chemistry

The use of sulfur based chemistry to attach organic species to metal surfaces has become very popular over the last decade [**2**]. This attachment is created by the formation of a covalent bond between sulfur and the metallic species. Metals for which this chemistry is commonly used on include Au, Pt, Pd, Ag, and Cu. A diagram demonstrating the reaction between a thiol (sulfur) end group and a metallic Au surface is given in Figure **2-10**. These types of reactions on a surface are commonly referred to a “self-assembling” because they form a semi-ordered monolayer on the surface [**2**].

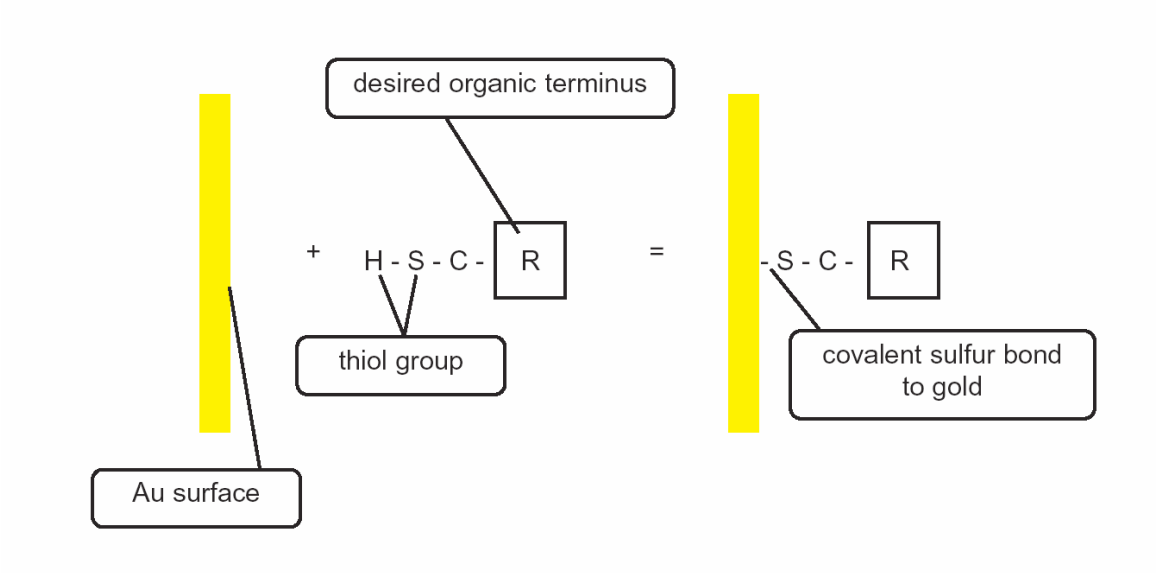

Figure **2-10**: A schematic of a sulfur bond linking an organic molecule to a metallic surface. The "R" group represents a variety of possible organic terminus groups.

Alkanethiols are useful for quickly determining the ability of a surface to run this type of chemistry. The molecule hexanethiol is shown in Figure **2-11**. A 100uM solution of this molecule in IPA was used to conduct tests on evaporated films to determine if they were functional to this chemistry. This molecule, when attached to a metal surface, creates a relatively hydrophobic surface. Various films were exposed to the hexane thiol solution for 1hr at room temperature and then rinsed for 5min in IPA and 5min in DI water. The films were tested afterward to see if they were hydrophobic using a quick contact angle observation. The contact angle of the edge of a drop of water on the films provided a quick yes or no answer to whether the surface was hydrophobic, indicating whether the reaction ran or not. The changes in contact angle were large, so these observations could be and were done by eye. This test was done

on various potential electrode metals and was used to determine the effect that the sacrificial layer removal process had on electrode functionality.

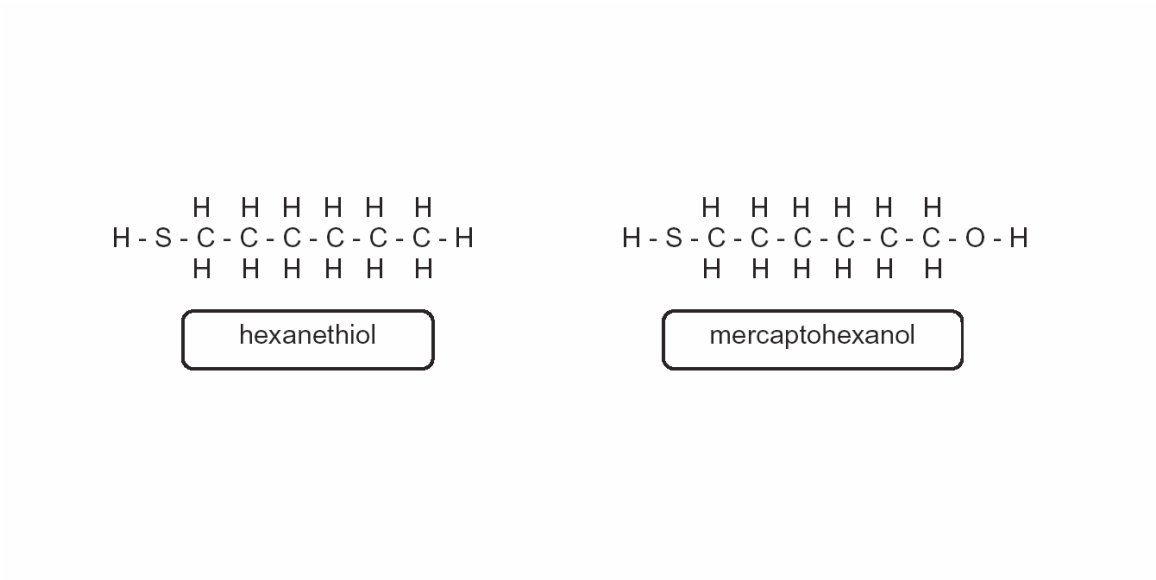

Figure **2-11**: Drawings of the two molecules hexanethiol and mercaptohexanol.

The electrodes within an actual nano-gap device were tested for functionality with a similar molecule, mercaptohexanol. This molecule is also shown in Figure 2-11. Mercaptohexanol was used because it can be dissolved in an aqueous solution, and this is required so that the epoxy encapsulation of the device does not degrade. For this experiment a 100uM solution of mercaptohexanol in DI water was exposed to the device for 4 hours, and then the devices were rinsed in DI water for 20min. Electrical measurements, discussed in the Section 2-3, were used to determine if the reaction ran on the electrodes within the device.

2.2.2 Bio-chemical Surface Modifications and Reactions

A novel linking scheme was developed to attach the small organic bio-molecule biotin to an electrode surface for use in the nano-gap sensor. This two step reaction is diagramed in Figure **2-12**. Here, cysteamine (Sigma) is used to modify the surface of the metal through a thiol reaction, exposing amine groups on the surface. Then a specially modified polyethylene glycol (PEG) polymer with ends terminated in biotin and a N-hydroxysuccinimide ester (Nektar Molecular Engineering Inc.) is attached to the amine groups. The PEG allows the biotin to react well with the protein streptavidin because of the spacing between the biotin and the metal surface. The length of the PEG spacer used was approximately 18nm (3400 Daltons). PEG with the ester modification but no biotin modification was also obtained for control experiments. PEG is commonly used for bio-coatings because it tends to prevent protein adhesion, which is good for the selectivity necessary for running the biotin-streptavidin interaction against controls.

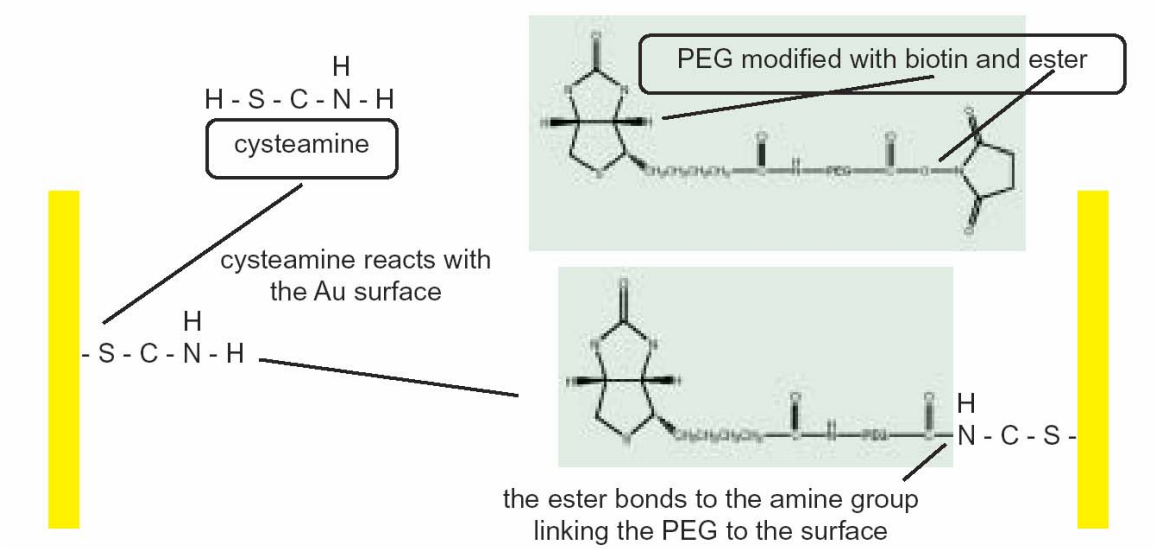

Figure **2-12**: Schematic showing the two step reaction to link biotin to a metal surface. The cysteamine is first reacted to the metal surface leave amine groups exposed. The ester group of the modified PEG then bonds to the amine groups.

The two steps of this linking chemistry were first explored on gold thin films. The cysteamine reaction was run at 100uM concentrations in DI water, methanol, and a mix of 90% IPA / 10% DI water. The gold samples were exposed to the solution for 4hr at room temperature and rinsed for 5min in DI water. The occurrence of the reaction against controls was obvious as the contact angle of the gold changed from about 80^{o} to about 25^{o}. The surfaces became hydrophilic because of the amine group. The reaction ran the best in the DI water/ IPA mixture, giving more uniform coverage and lower contact angles. The ester of the modified PEG degrades when exposed to water, so the PEG was aliquotted into 10mg vials and vaccum packed until use. The modified PEG molecules are stable for about 1hr in a pH 8 buffer, so the solution must be prepared immediately before use. Once bonded to the amine groups, the PEG is

stable for days in an aqueous state. To attach the PEG to the cysteamine modified surfaces, the PEG was hydrated in a .1M pH 8.0 phosphate buffer to a concentration of 1mg/ml and was allowed to react with the surface for 1hr. After a 5min DI water rinse, the contact angle of films were observed. The PEG modifications (biotin PEG and non-biotin PEG) caused the films to become more hydrophobic over control films placed in buffer alone. The surface of the films with the PEG modifications also felt oily to the touch. These observations in contact angle do not prove the reactions occur as designed, so the selectivity of the films for binding streptavidin was explored.

Streptavidin, a protein, binds well to the biotin molecule. Streptavidin coated nano-particles (20nm, British BioCell intl.) were used to test the biotin attachment chemistry above. The as received nano-particles were diluted 100:1 in a pH 7.5 standard Phosphate Buffered Saline (PBS) solution prior to reacting with the surfaces. The nano-particle solution was applied to samples with a cysteamine modification, a PEG modificiation, and a biotin-PEG modification. After reacting at room temperature for 30min, the samples were rinsed for 30min with the PBS solution. The samples were dried with a nitrogen gun, and were analyzed for the presence of the nano-particles with a field emission scanning electron microscope (FESEM, LEO 1530, Leica Inc.).

The above reactions were run on the electrodes within nano-gap device in a similar manner. The reaction times for the cysteamine and PEG chemistries were the same as on the deposited films. The cysteamine reaction was performed prior to device encapsulation, because it is run in an IPA solution

which may damage the encapsulation materials. For the streptavidin-biotin reaction, a 1hr reaction time was performed with a 1hr rinse with PBS. A nano-particle free streptavidin solution (Sigma) was also used to react with biotin inside the nano-gap deives. The presence of streptavidin and streptavidin coated nano-particles within the device electrodes was determined with electrical measurements only, because SEM is not possible on the enclosed deivces.

2.3 Electrical Measurements

The nano-gap device was analyzed using DC and AC electrical measurements. All DC and quasi-static experiments were performed with a Hewlett Packard 4145 semiconductor analyzer, and all AC impedance measurements were performed with a Hewlett Packard 4284 impedance analyzer. The device was connected with shielded probes on a micromanipulator system (Micromanipulator Inc.).

AC measurements were used to determine the impedance characteristics of the device under various conditions. The measurements were taken between 100 and 1MHz at an AC amplitude of 50mV. Calibration to eliminate probe impedance was performed on devices with the bottom electrode only for the open compensation and on devices that did not have the sacrificial layer removed for the short compensation.

Quasi-static measurements were used to explore the device current voltage characteristics. Sweep measurements were taken from 0-35V at a rate of 100mV/sec.

A three probe configuration with the HP 4145 was used to bias the electrodes with respect to the solution. This was performed to electrically migrate nano-particles in and out of the device electrode gap. For these experiments, both of the electrodes were set to ground. The third probe was connected to a tungsten probe immersed into the solution within the encapsulation well and was biased with respect to the grounded electrodes.

2.4 References

1. W. J. Nam, “Molecular Scale Gap Sensors Fabricated Using Sacrificial Layers and Self-Assembly,” dissertation, University Park: Penn State University, 2003.

2. A. Ulman, “Formation and Structure of Self-Assembled Monolayers,” Chemistry Reviews, vol. 96, pp.1533-1554, 1996.

Chapter 3

Experimental Results

This chapter provides results regarding the nano-gap sensor device fabrication, chemical assembly, and the ability to use the device to detect biological interactions. The following sections will detail results on device yield/integrity measurements, device functionality (the ability to tailor the surface of the electrodes with self-assembling chemistries), and the device use as a biological interaction detector. Many secondary observations which are important for device and experimental understanding will also be reported. It will be shown that the nano-gap sensor has been improved over prior work in our group [**1**], that a new selective and robust surface chemistry has been developed, and that the combination of these allow for the electrical detection of chemical and biological species. Following the presentation of these results, a theoretical discussion of key results is given in Chapter 4.

3.1 Device Yield and Integrity

Two important characteristics of the nano-gap sensor devices are their integrity and yield. Device integrity refers to the device's resistance to electrode collapse, which is an important indicator of device robustness and is necessary for types of detection measurements detailed in Section **3.2.4**. Device yield

refers to the percentage of devices that are defect-free and working properly, which provides a feel for device reproducibility and manufacturing robustness. Results exploring these aspects are given below for a variety of device electrode and sacrificial layer materials. Also given are observations on the effects of the capping layer and water inside the device on these measurements.

3.9.1 Device Breakdown

Device integrity was examined with device "breakdown" experiments. Device breakdown occurs when the device irreversibly changes from a high resistive state to a low resistive state. Typical trans-gap resistances in air before breakdown are 27Gohms for devices using a quartz wafer substrate and .7Gohms using aluminosilicate substrate. These values are effectively open-circuit. After breakdown, device resistances approach that of the contact leads, ranging between 1 and 10kohms. The low resistance state is caused by shunting the top and bottom electrodes, which most likely occurs through a mechanism of electrode collapse. This collapse may be induced with the application of voltage across the two electrodes. Devices with high breakdown voltages (the voltage at which the device breaks-down) are desired, because a strong device will not breakdown during handling and will allow for high voltage sweep experiments. During handling static charge must be controlled, because devices, especially weak devices, can breakdown due to charge buildup on the insulating substrate.

Results of the measured breakdown voltage for various types of devices are presented in Table **3-1**. This table shows that the gold electrode devices are, in general, more susceptible to breakdown than the platinum devices. The ease of electrode collapse in gold electrode devices was suspected to primarily arise from the poor adhesion of gold to most surfaces, even with a chrome adhesion layer to silicon dioxide. The strength and stiffness of the capping layer, the rigidity and mechanical strength of the electrode metal, and electromigration were considered secondary effects. Gold adhesion to surfaces is poor because it does not form an oxide or alloy easily with other metals. Compositionally graded gold films were explored as an approach to this problem. By grading the composition of the films during deposition, there is no sharp interface between the adhesion film (Ti or Cr) and the gold. The results show that a hybrid device with a bottom electrode of platinum and a top electrode of a graded gold-platinum layer on a titanium adhesion layer has the strength (breakdown at 27V) of a platinum device. A device with Au graded with Ti electrodes was also fabricated. The titanium-gold system was chosen over chrome-gold because titanium has a more stable evaporation rate than chrome, and therefore, is easier to create a graded film in our system. Unfortunately, devices with these electrodes had unacceptable breakdown characteristics, as shown in Table 3-1. The reason for this poor strength will be discussed in Section 4-1-1.

Table **3-1**: Device breakdown voltages of various device material systems

Device Style	Average Breakdown Voltage (minimum 2 devices)
Platinum electrodes / Nickel sacrificial layer – prior work [**1**]	25.8
Platinum electrodes / Nickel sacrificial layer – this thesis	34
Platinum electrodes / Copper sacrificial layer	28
Gold electrodes / Nickel sacrificial layer	20
Graded Gold-Platinum top electrode with platinum bottome electrode / Nickel sacrificial layer	27
Graded Gold-titanium electrodes / Nickel sacrificial layer	<3

Although the typical gold devices have a reasonable breakdown voltage of 20V, their current-voltage characteristics are poor compared to the platinum devices. This is shown in the breakdown curves provided in Figure **3-1**. Here, the graphs show that a typical gold electrode device has a fluctuating current at voltages above 5V. The platinum electrode devices have a stable high resistance state. Figure 3-1 also shows the high resistance state differences between the Pt-Ni (platinum electrode – nickel sacrificial layer) devices which were fabricated on quartz, and the Pt-Cu and Au-Ni devices which were fabricated on aluminosilicate glass.

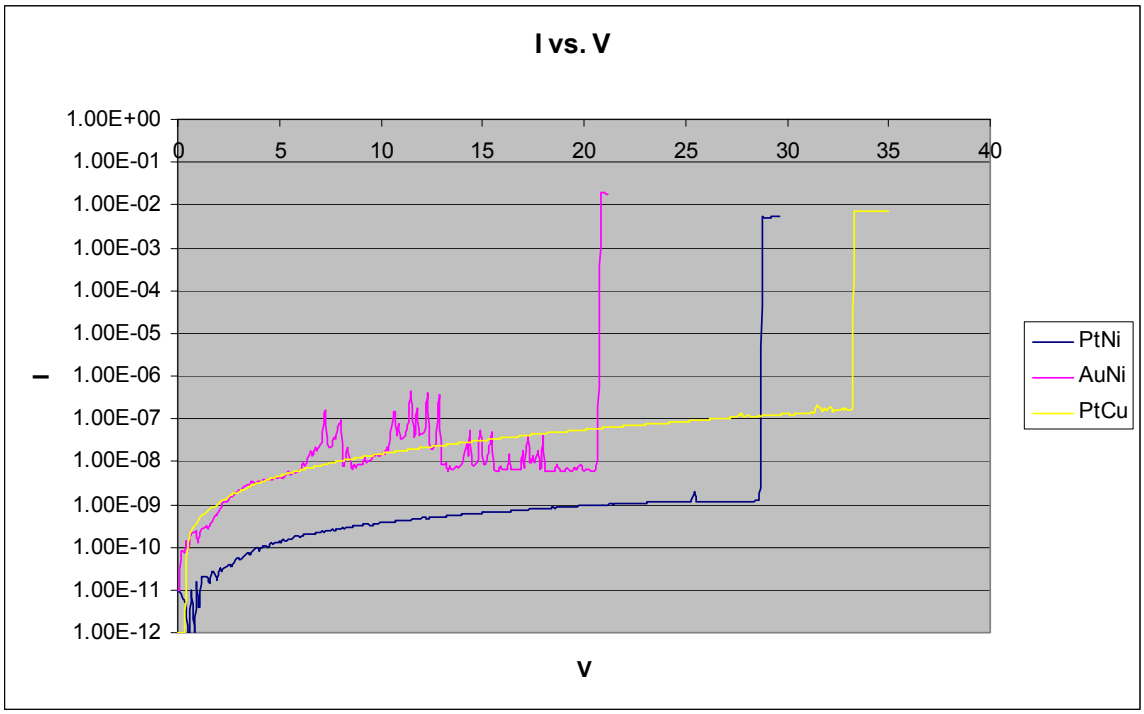

Figure **3-1**: Current voltage sweeps taken during breakdown experiments on platinum electrode / nickel sacrificial layer (PtNi), platinum electrode / copper sacrificial layer (PtCu), and gold electrode / nickel sacrificial layer devices(AuNi).

3.9.2 Device Yield

High device yield is an important measure of the robustness of the manufacturing techniques used in device fabrication. Using our current manufacturing techniques, devices fabricated with a nickel sacrificial layer have an excellent yield, i.e., about 95%. The yield was the same for platinum and gold electrode devices. Upon operation however, the gold electrode devices quickly begin to fail due to static buildup. Platinum electrode devices with a copper sacrificial layer, including those created on a wafer that also had high yield nickel

sacrificial layer devices, have a moderate yield of approximately 75%. This will be discussed in Section 4-1-2.

3.9.3 Access Hole Etching Study

Without a second channel structure incorporated into the device design, chemicals must diffuse from the access hole through the nano-channel to get to the device electrodes (see Figure 1-8). With a 50um long nano-channel on either side of the electrode gap, small molecules can diffuse in relatively fast (<5min), based on a simple diffusion model; however, large molecules such as proteins may take 30 min or more. Therefore, it is desirable to have the shortest nano-channels possible. The typical device design has a 10um thick capping oxide, and with isotropic etching of the access holes, this inherently limits the access channel length.

An access hole etching study was done to determine the etching characteristics of the deposited oxide and quartz substrate and find the shortest nano-channel length available with this design. Figure **3-2** shows pictures of a Pt-Ni (platinum electrodes – nickel sacrificial layer) device with increasing access hole etch times. Here we see that the upper rim of the access hole approaches the device electrodes with approximately 12 min of etch time. This results in the shortest nano-channel length possible being 30um in length. Surprisingly, the strength of the device in breakdown experiments was roughly constant with the increased etching time. The 12 min device had a breakdown voltage of 28.5V,

even with the observed reduction of capping layer thickness over parts of the electrodes. This observation lead to the thin capping layer study below, because it indicates that the electrode adhesion to the capping layer is of primary importance.

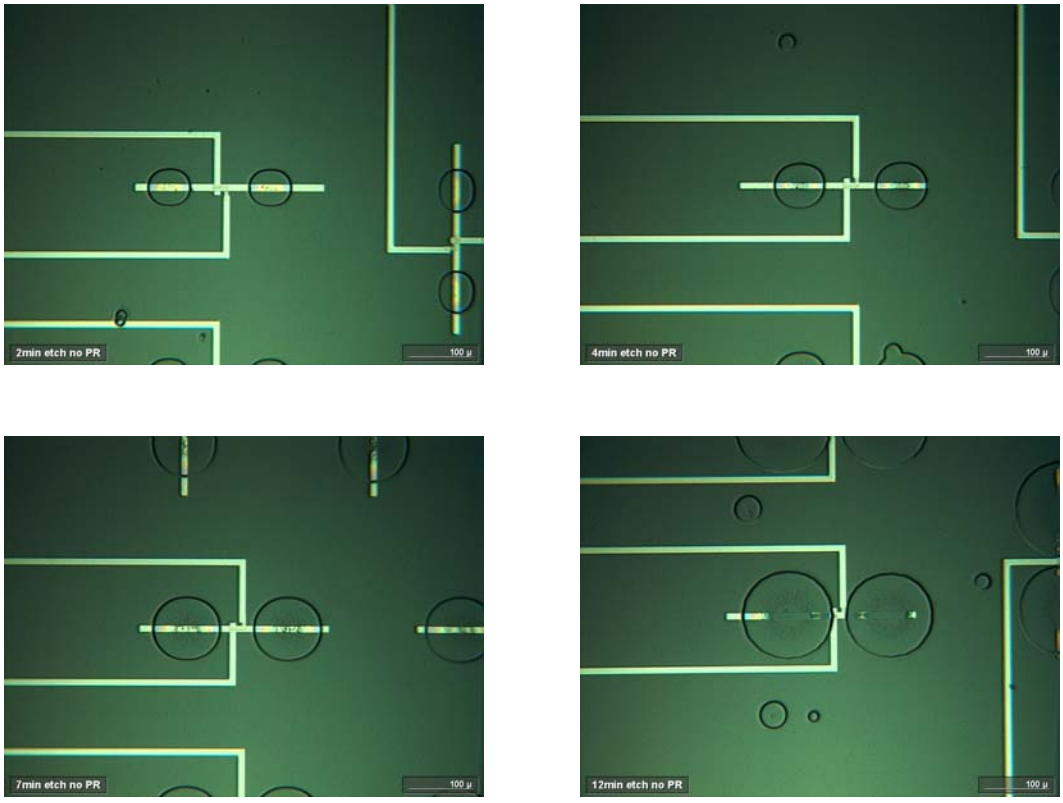

Figure **3-2**: Progression of access hole etching at (a) 2min, (b) 4min, (c) 7min, and (d) 12min.

Unfortunately, the copper sacrificial layer devices do not offer the flexibility of increased etching times, because the copper etches in hydrofluoric acid, destroying the device by etching into the electrode structure during extended access hole etching.

3.9.4 Thin Capping Layer Effect on Breakdown

The effects of a thin capping layer on device strength were explored, because a thin capping layer would translate to less cost. For this study, a 4um oxide was deposited on platinum devices, and breakdown measurements showed that the average breakdown was equivalent to the 10um capping layer devices. This shows that a thinner capping layer may be used without degradation of device strength. Unfortunately, the thin capping layer has extreme effects on the AC impedance characteristics of the device, which will be shown in Section **3.10.1**.

3.9.5 Water Effects

The presence of water within the device can be detected electrically but not optically. Avoiding the presence of water requires an extended period of time for devices to dry out after a rinsing step, because of the capillary effects of the nano-channel. At room temperature, devices may take between 3 and 24 hours to dry completely depending on the surface chemistry of the channel walls. For example, devices whose substrate and therefore, nano-channel walls were prepped with NanoStrip^{TM} had with highly hydrophilic channel surfaces and required up to 24 hours to fully dry. Using a vacuum dry, most devices dry within 10min, and a 20min vacuum dry ensures that all devices, regardless of the surface conditions, are water-free. Of course there will always be remaining mono-layers of water on all glass surfaces, but electrically, such devices will

appear water-free. The effect that residual water has on a breakdown sweep is shown in Figure **3-3**. The water gives rise to an electrochemical current until all of the water fully vaporizes. Once dry, the voltage sweep appears the same as a dry device; however there is damage caused to the electrodes which lowers the average breakdown voltage of the device.

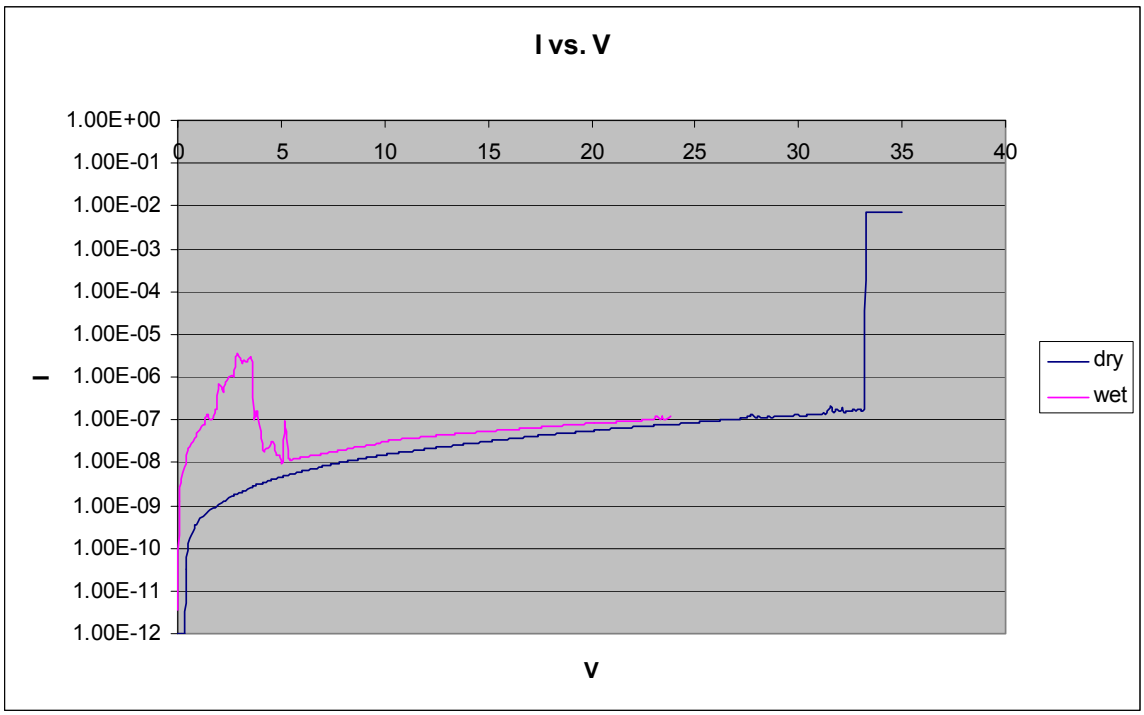

Figure **3-3**: Breakdown sweep characteristics of a dry and partially wet device.

3.10 Device Functionality and Use as a Biological Interaction Detector

To complete the goals of this work, the devices must not only have good strength, but also must be functional, allowing reactions to take place on the electrode surface. Device functionality was explored using water contact angle

observations on deposited films and monitoring AC impedance changes of devices. It was found in prior work [**1**] that AC measurements were useful in monitoring self-assembling reactions of alkanethiols within the electrode gap, so this method and these molecules are used here to evaluate electrode and device functionality. We also report the monitoring of the newly developed biological chemistry and biological interactions within the device with AC impedance and DC breakdown experiments. In the following section typical impedance measurements from the nano-gap devices are given along with typical parasitic effects, so the impedance data that follows can be better understood.

3.10.1 AC Impedance and Parasitic effects

High frequency AC impedance measurements provide information on the state of the electrode gap and changes occurring on the electrodes. Typical resistance and reactance plots versus frequency of a device filled with a 1M salt buffer are shown in Figure **3-4**. After filling the device with a solution, the impedance values change quickly at first and the slowly reach a steady state over a few minutes. Therefore all measurements are taken after waiting approximately 5 minutes for the values to settle. Impedance values do vary slightly from device to device, as the top electrode has varying area (approximately 20% across a wafer) on different devices because of lithography registration errors. Note from Figure **3-4** that the impedance cures do not mach

a simple capacitor circuit model with a series or parallel resistor. The circuit model for this device will be discussed in Section 4.2.

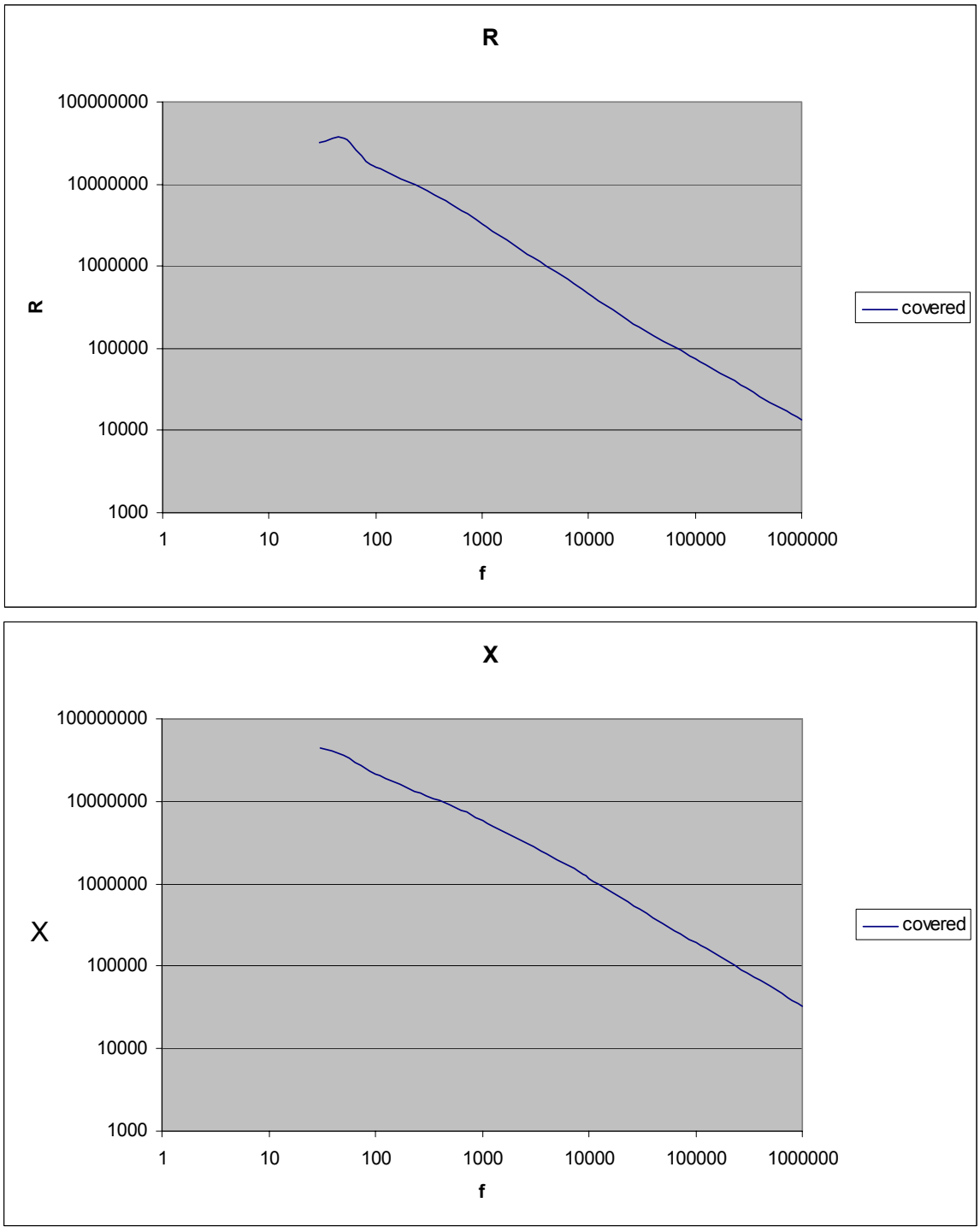

Figure **3-4**: Typical resistance and reactance impedance characteristics versus frequency for a 50nm nano-gap device.

The parasitic impedance from the contact leads has significant impact on the impedance characteristics of this device. The parasitic impedance arises from the pathway created from the contact leads through the capping oxide to the conductive solution. By covering parts of the electrodes with epoxy to reduce the residual capacitance, a trend of electrode coverage and its effect on impedance can be shown as in Figure **3-5**. With a 10um oxide the figure shows that the parasitic impedance primarily effects the characteristics of the device in the frequency range from 10 Hz to 10 kHz. In order to eliminate irreproducibility due to packaging errors, the measurements for the rest of the study will be restricted to the frequency range between 10 kHz and 1 MHz. The parasitic impedance of the 4micron thick capping layer devices dominated the device characteristics at all frequencies, eliminating the ability to do AC impedance monitoring. Therefore all impedance results presented are using 10um capping layer devices.

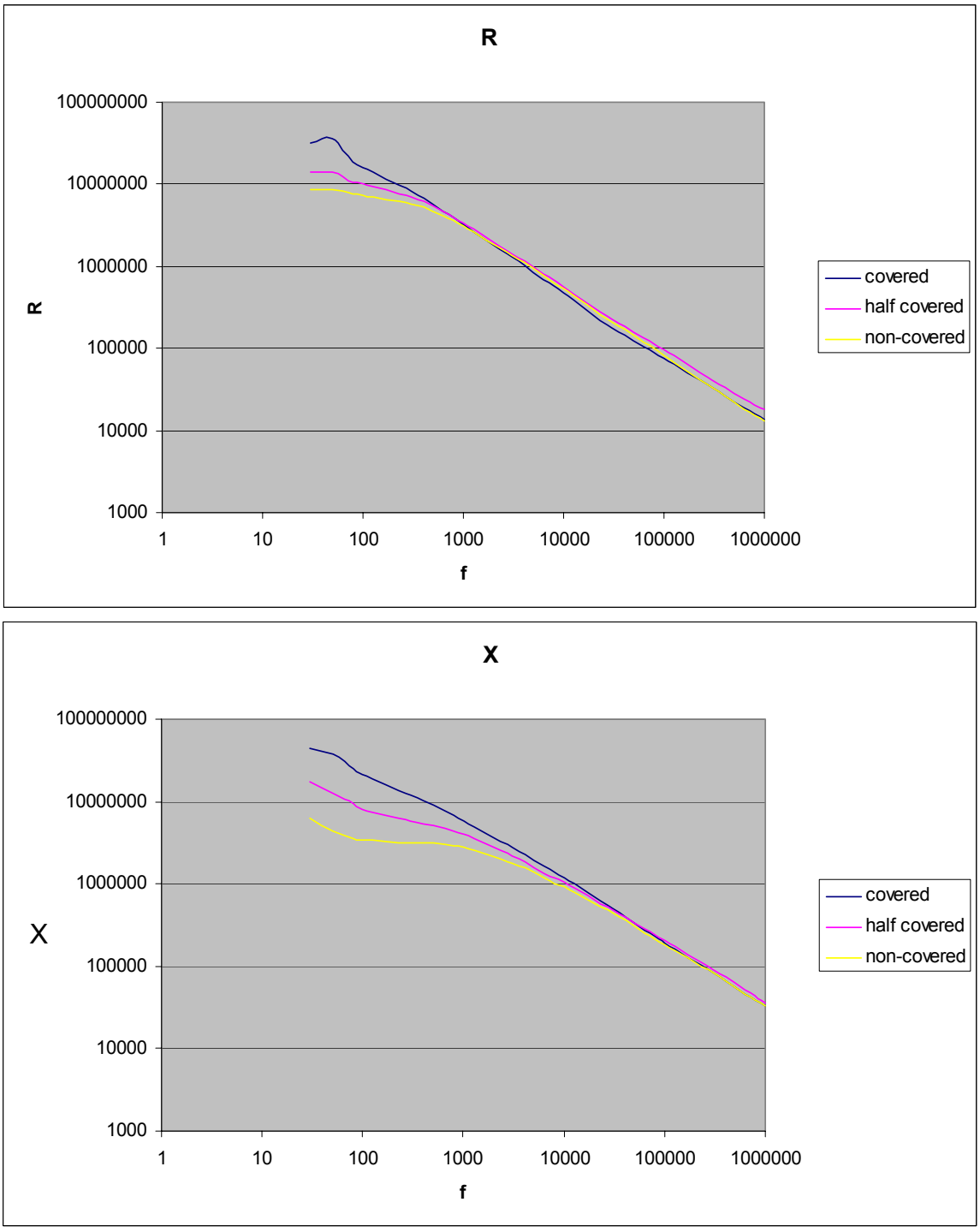

Figure **3-5**: Impedance characteristics with electrodes that are insulated (covered), partially insulated, and non-insulated (non-covered) with epoxy.

Impedance measurements can also be used to determine the state of the device during drying. An example of the impedance characteristics of a dry and partially dry device are shown in Figure **3-6**. These differ from the characteristics of a fully wet device shown in Figure **3-4**. A circuit model presented in Section 4.2 explores the partially dry device characteristics.

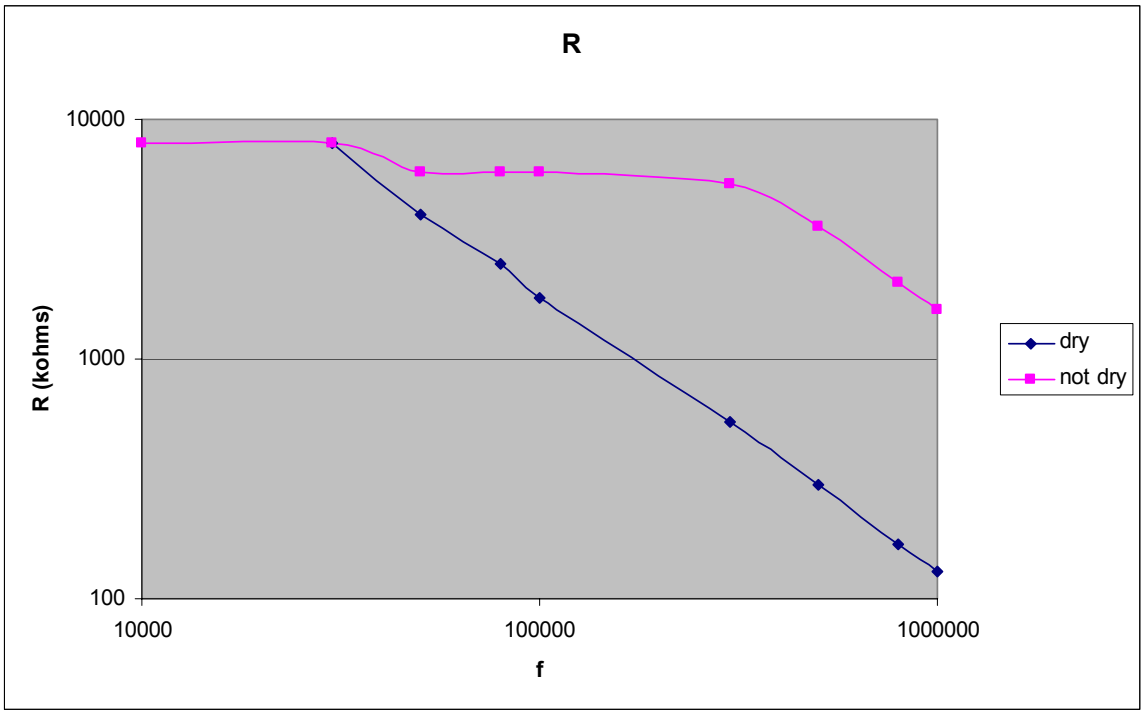

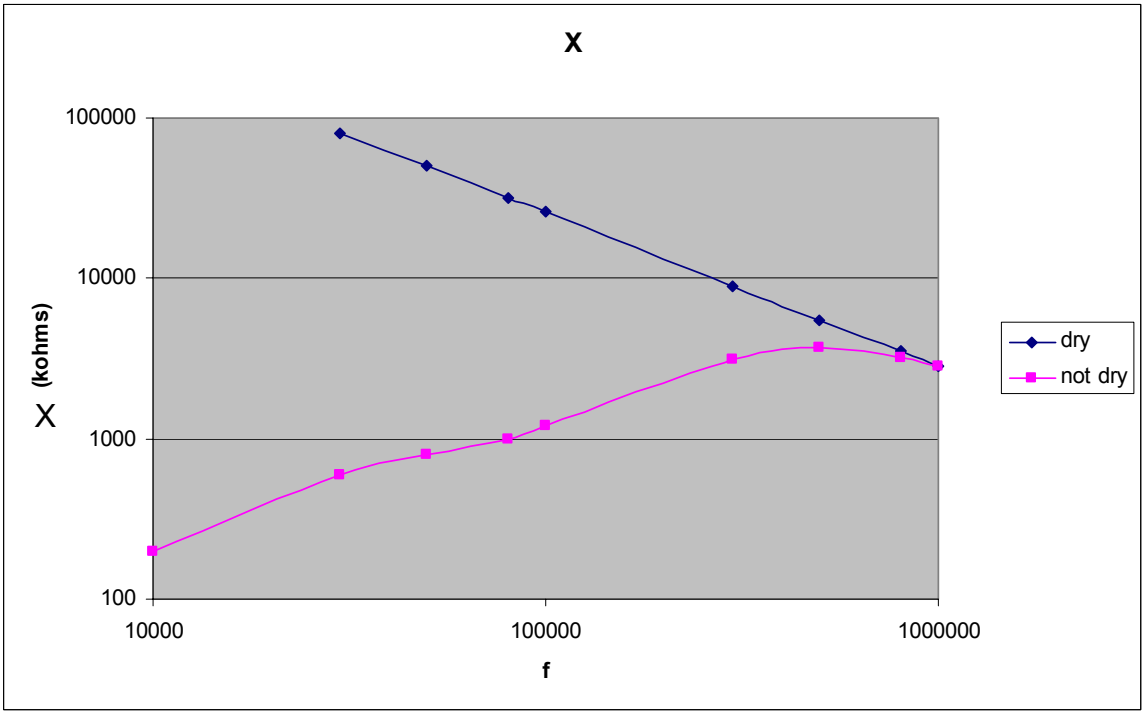

Figure **3-6**: Impedance characteristics of a dry and partially dry device.

3.10.2 Device Functionality Tests

Before reporting the results from functionality tests on the various device material configurations, it is necessary to discuss experiments which led to the materials choices. It is well known that platinum forms a sulfur bond with organics enabling self-assembling chemistries [**2**]. The fact that the platinum devices with a nickel sacrificial layer are not functional [**1**] raises questions and inspired a study using simple deposited films on glass substrates. Here the sacrificial layer effects on the electrode chemistries are explored.

3.10.2.1 Deposited Film Self-Assembly Experiments

The first test performed to explore deposited film surface chemistry looked at the effects of a nickel film deposited on gold and platinum films. This was done to explore the impact that the removal of the Ni sacrificial layer had on the ability of the underlying metal electrode to form sulfur surface chemistry bonds. In this study, Ni films were etched away from the platinum and gold films in the same manner as the sacrificial layer removal step in device fabrication. Then, along with bare platinum and gold controls exposed to the etching solution, a self-assembling hexanethiol reaction was performed, which should produce a hydrophobic surface. After the reaction, the control samples were very hydrophobic, with contact angles greater than 90^{o}. However, both the gold and platinum films that had nickel etched away from their surface were hydrophilic, indicating that the reaction did not run. This indicates that for the gold devices to

show chemical functionality, as in our group's previous work [**1**], the top electrode is serving as the only functional electrode.

It was also observed that when the Au/Ni/Au layer stack is formed in device fabrication that the top Au layer scratches off very easily from the Ni layer. The poor adhesion of the top Au layer indicates no intermixing of atomic species of the two metals (alloying). The bottom Au/Ni interface is strong and must alloy to some extent during the Ni deposition. In the Pt/Ni/Pt layer stack, all films adhere well to each other, which is consistent with the well-know fact that Pt alloys with other metals very easily during deposition [**3**]. Ni does not bond to thiol chemistry, and alloys of Pt and Au would probably not allow thiol chemistry to run, which is what we see above. These observations lead to the trial of different sacrificial materials (copper and palladium) and a different electrode material (palladium).

Palladium was explored as an electrode material because it has good strength, chemical resistance, and it enables thiol chemistry. Unfortunately, the palladium behaved in the same manner as the gold and platinum, by not reacting with the hexanethiol after Ni etching, because of alloying. The palladium was also explored as the sacrificial layer on the platinum films, because, if an alloy was formed, both metals would be able to form a thiol bond. Nickel etch type I was used to etch the palladium, since it was found to be selective over platinum. Bare platinum exposed to this etchant reacted with the thiol, but after the palladium was etched away, the film would not. The exposed palladium in the platinum alloy, after exposure to the etchant, must prevent thiol-bond formation.

A copper sacrificial layer was also explored with much better results. Copper was attempted because it forms a thiol-bond and etches very easily, which is important for a sacrificial layer. The copper did not adhere strongly to the gold, indicating little alloying, and after etching, enabled the formation of a thiol based monolayer. After etching the copper from the platinum, self-assembled monolayers were also formed. With the platinum, however, the films were very hydrophilic after Cu etching. This also occurs with bare platinum exposure to the TFB type Ni etchant. After an IPA rinse the Pt films change into a surface state with a contact angle similar to the as-deposited platinum. This indicates that a non-water soluble residue is present on the surface, probably the surfactant which is part of the etch chemistry. The presence of this surfactant is not a problem, because most thiol chemistry runs in solvents. The copper also etched very quickly (<10sec) in Nickel etchant type TFB, which is promising for the etch step within the device.

A summary of the results from these surface chemistry studies is given in Table **3-2**. From this work, we report that a copper sacrificial layer enables at least the bottom electrode to be functional for Au and Pt devices, which is an improvement on prior work. The results of self-assembly within these dirrerent devices are covered in the next section.

Table **3-2**: Summary of deposited film studies for thiol-based chemical functionality on deposited films, mimicking the bottom electrode of a nano-gap device.

Electrode Material	Sacrificial Material	Etchant	Functional (y/n)
Au	Ni	Ni etch type TFB	No
Au	Cu	Ni etch type TFB	Yes
Pt	Ni	Ni etch type I	No
Pt	Ni	Ni etch type TFB	No
Pt	Pd	Ni etch type I	No
Pt	Cu	Ni etch type TFB	Yes
Pd	Ni	Ni etch type TFB	No
Pd	Cu	Ni etch type TFB	Yes

3.10.2.2 Device Functionality Testing

Impedance measurements were used to probe the functionality of the electrodes inside the device. The impedance changes of the device after exposure to a self assembling chemistry are difficult to interpret, but can be useful in determining whether reactions ran or not if controlled properly.

Typical changes in impedance for a gold electrode device (nickel sacrificial layer, AuNiAu devices) after assembly of a mercaptohexanol are shown in Figure **3-7**. This figure shows that over the 10kHz to 1MHz frequency range, the resistance and reactance both increase with the presence of the monolayer. The possible reasons for these changes will be explored in the next chapter; however, the change with respect to the control device, which showed substantially no change in impedance characteristics, gives a strong indication that the reaction has occurred.

Surface coverage of self-assembling monolayers under most conditions tends to be non-uniform [**2**], and this non-uniformity is observed through varying changes in impedance from device to device in assembly experiments. Figure **3-8** demonstrates this point. Here, the average % change in impedance for a sample of AuNiAu devices after mercaptohexanol assembly is shown. Plotted are both the average % changes in impedance and error bars indicating the high and low values of the set. The changes observed in control devices exposed to the buffer solution without mercaptohexanol are also shown. There is a clear change between the two sets of devices after monolayer formation even with the large variation of changes in the monolayer coated devices. This means by of representing impedance data in Figure **3-8** for the purposes of monitoring surface coating reactions is appropriate for two reasons: (1) it eliminates the variability in initial impedance parameters by representing changes in impedance, and (2) it averages changes from device to device to better represent overall changes induced by the monolayer.

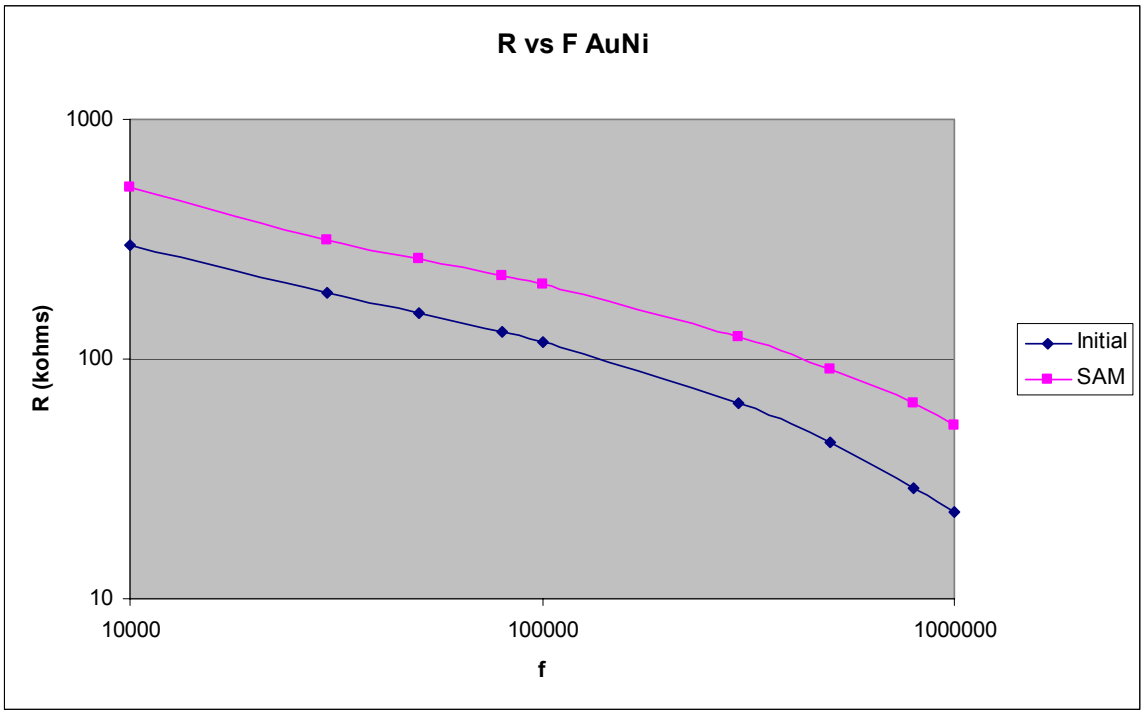

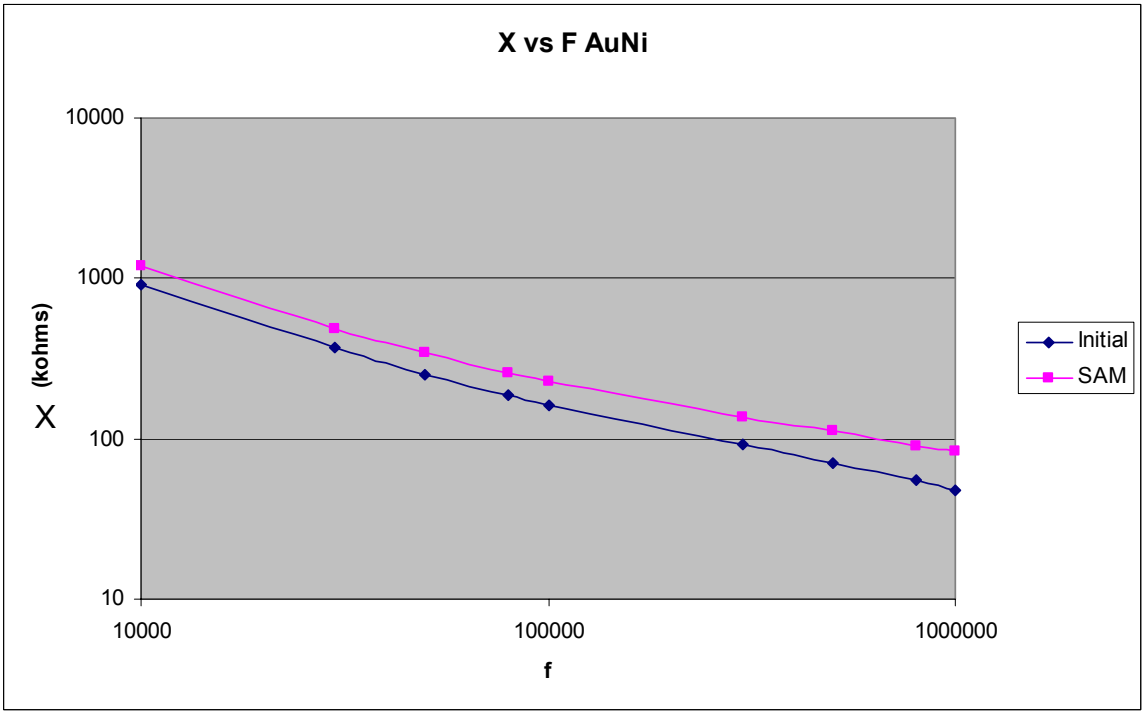

Figure **3-7**: Impedance curves for an Au electrode device showing the change in impedance characteristics after the assembly off a monolayer (SAM).

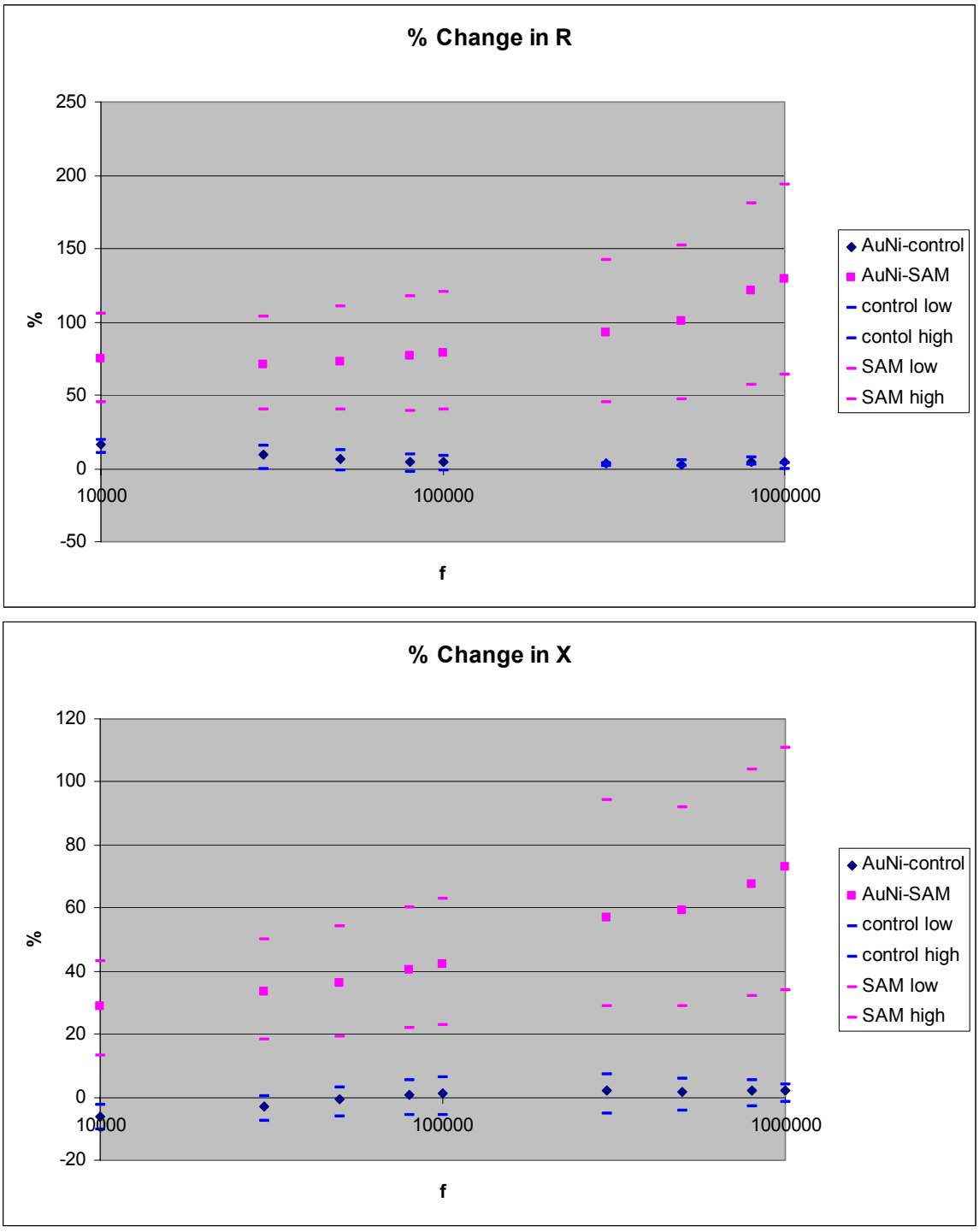

Figure **3-8**: Percent changes in impedance characteristics of a set of devices after exposure to a control solution (control) and a mercaptohexanol solution (SAM). The high and low values from the set of devices are also shown.

Platinum devices with a copper sacrificial layer (PtCuPT devices) also showed the ability to chemically functionalize at least one of their electrodes. The platinum devices fabricated in our prior work with a nickel sacrificial layer did not [**1**]. Typical impedance changes in PtCuPt devices after an IPA rinse and mercaptohexanol monolayer formation are shown in Figure **3-9**. One difference between the AuNiAu devices and the PtCuPt devices is the change in device parameters after a solvent (IPA) treatment. As discussed in Section **3.10.2.1** an IPA rinse changes the Pt surface chemistry, and this is observed in device impedance measurements as well. After the IPA rinse, the device has stable impedance measurements and self-assembling experiments can be performed. The % impedance changes due to mercaptohexanol assembly for the PtCuPt and AiNiAu devices are shown in Figure **3-10**. From the plot, it is apparent that PtCuPt devices do not exhibit changes as dramatic as the AuNiAu devices, but it is clear that the reaction ran on the PtCuPt devices. This is an important result, because it demonstrates that platinum electrode devices with their excellent mechanical strength and with chemical functionality can be fabricated.

Surprisingly the devices with a top electrode comprised of graded Au and Pt did not show chemical functionality through impedance changes. The devices with graded Au into Ti were not robust enough to perform impedance experiments.

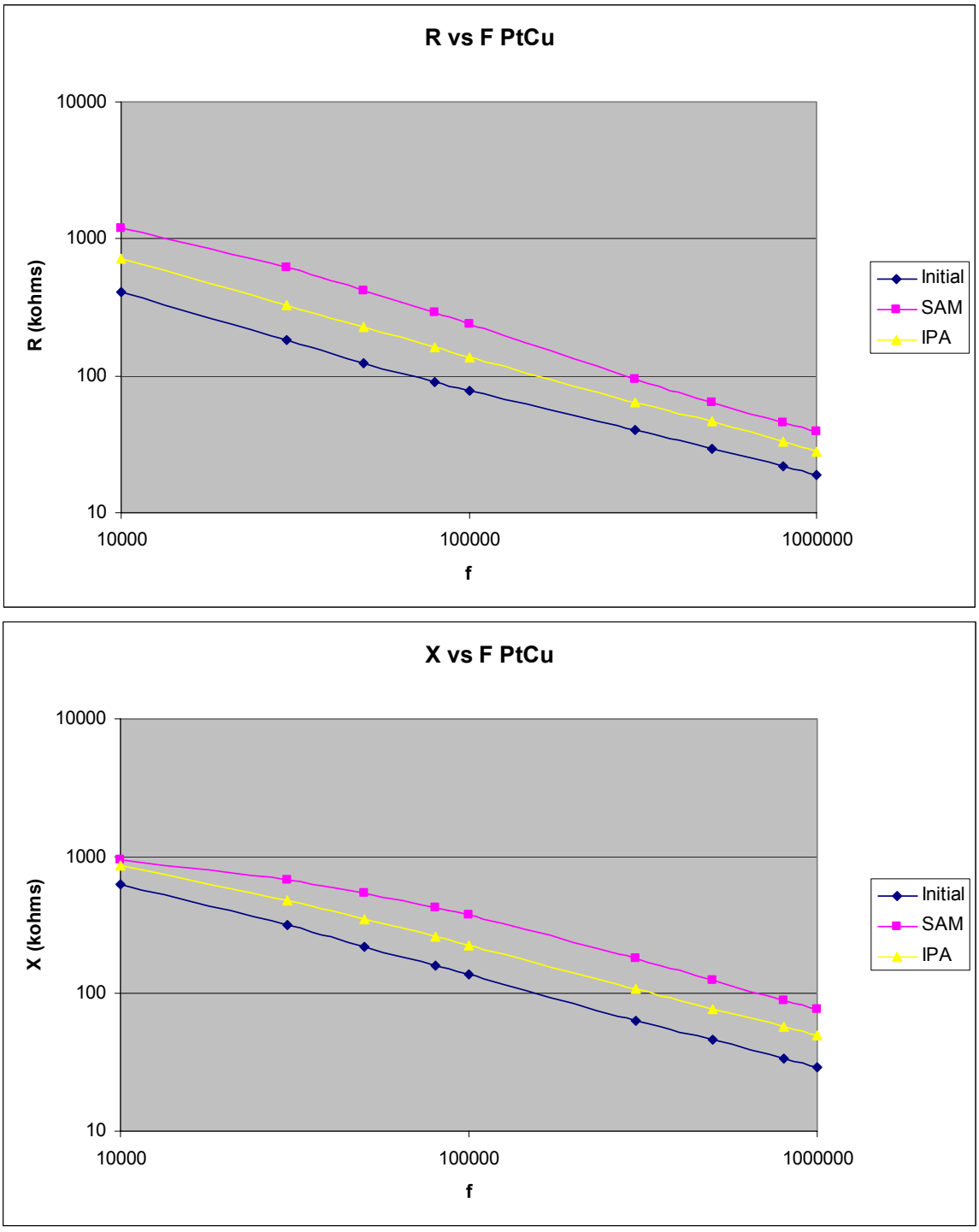

Figure **3-9**: Example impedance changes from a PtCuPt device before (initial) and after (IPA) an IPA rinse and self-assembly of mercaptohexanol (SAM).

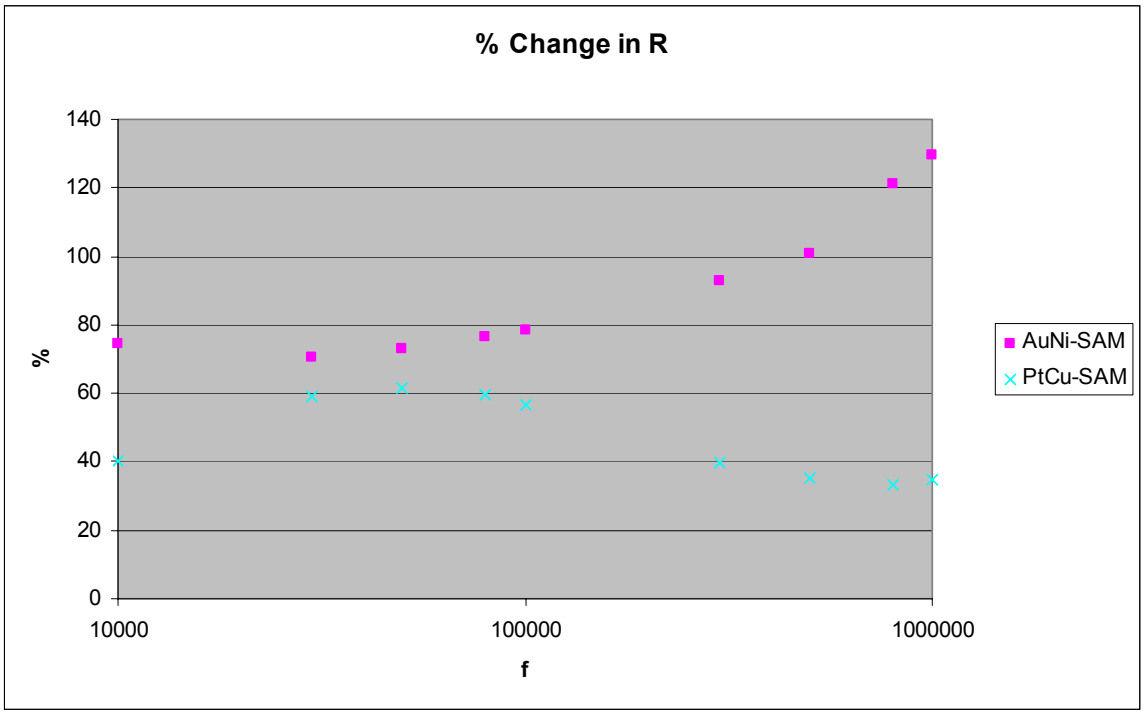

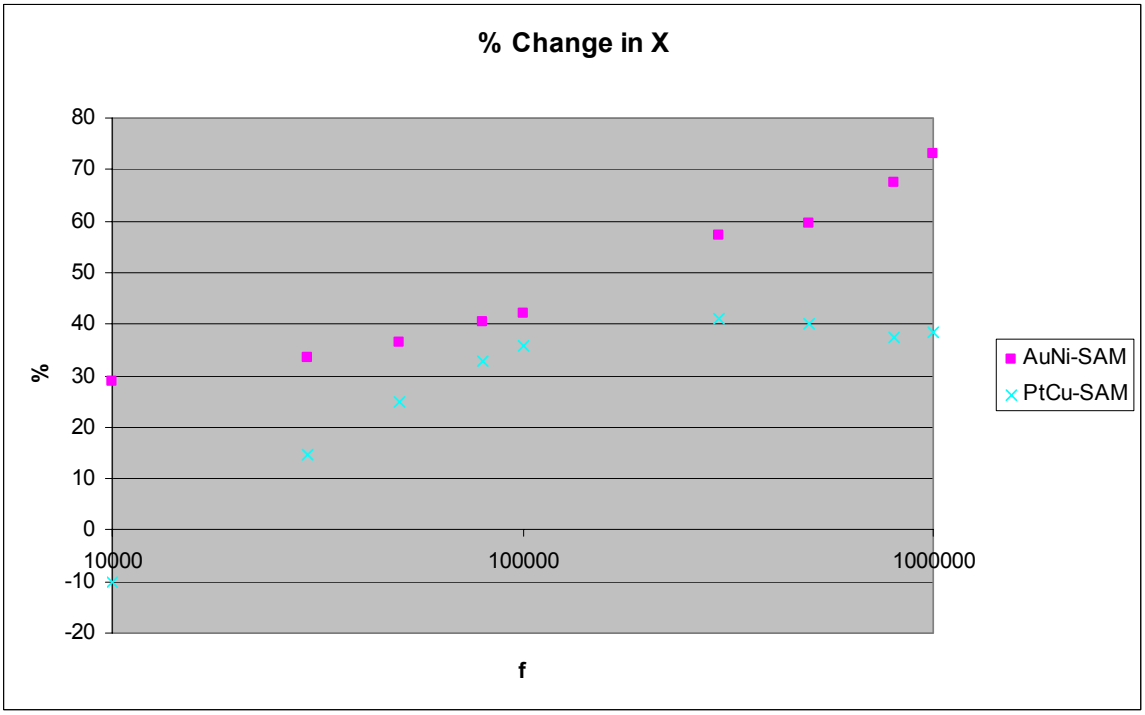

Figure **3-10**: Average percent changes in PtCuPt and AuNiAu devices after mercaptohexanol monolayer formation.

3.10.3 Monitoring Bio-chemical Self-Assembly

Impedance measurements were also used to determine if the two step biological surface modification could be monitored. The two step reaction involves a cysteamine reaction to the surface and a PEG attachment to the amine terminus of the cysteamine as discussed in Chapter 2. This reaction was also studied on deposited films with contact angle measurements. On deposited films, the cysteamine reaction caused the water contact angle to change from approximately 85^{o} to 25^{o}, changing the gold surface to hydrophilic. This is as expected for an amine terminated surface. Gold electrode devices (AuNiAu) were used to check for changes in impedance after the cysteamine step, and no substantial change was detected. This did not indicate, however, that the reaction did not run, only that the surface modification did not effect the impedance characteristics. After the PEG reaction (for both the biotin modified PEG and the non-biotin PEG) the deposited films changed to have an approximately 75^{o} contact angle and were greasy to the touch, indicating that the reaction ran. The changes detected after PEG assembly within the device are shown in Figure **3-11**. This data also gives strong evidence that the reaction took place when compared with that of the control device also shown in Figure 3-11, which had a cysteamine treatment and was exposed to reaction buffer without PEG.

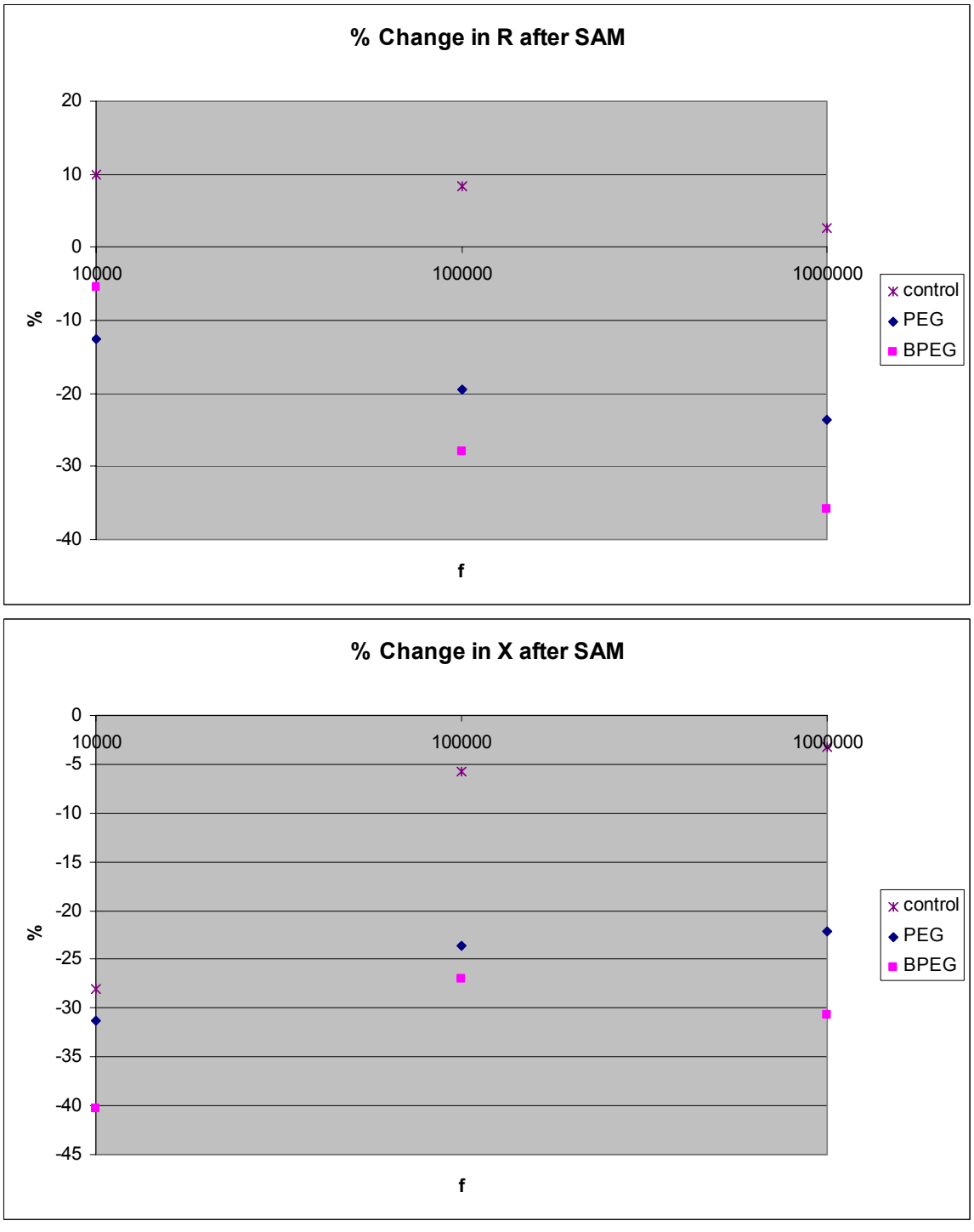

Figure **3-11**: Average changes in impedance after surface linking of a PEG molecule with and without a biotin terminus. A control which was exposed only to the reaction buffer solution is also given.

3.2.4 Detecting Biological Interactions

Both AC impedance and DC breakdown measurements were used to monitor the interaction of streptavidin with the biotin terminus of the PEG modified electrode. Prior to testing the devices, streptavidin binding was studied on deposited films with streptadivin coated Au nano-particles so that the results could be visualized with SEM. Results from a hybridization experiment, monitored by SEM, with streptavidin nano-particles on a cysteamine terminated control surface, a PEG surface, and a biotin-PEG surface are shown in Figure **3-12**. The excellent selectivity of the surfaces to the biotin-streptavidin interaction is apparent in these images, and a summary of the bead densities is given in Table **3-3**. Virtually no nano-particles adhered to the PEG surface. This shows the ability of the PEG to mitigate against streptavidin attachment. The high density of nano-particles on the biotin-terminated surface confirms the efficacy of the two step biotin-PEG reaction and is effectiveness in bonding with streptavidin coated nano-particles. To the writer's knowledge, this is the first time this specific sequence of surface chemistry has been demonstrated for the biotin-streptavidin interaction.

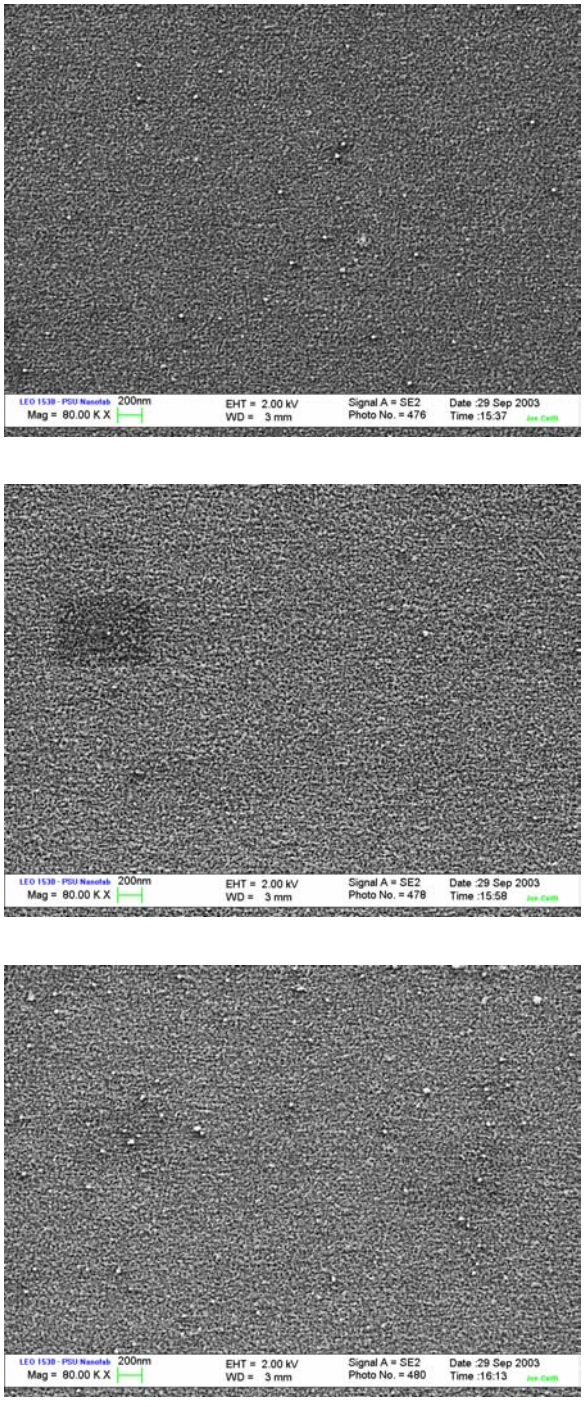

Figure **3-12**: SEM images of streptavidin nano-particles bound to a cysteamine terminated surface (top), a PEG terminated surface (middle), and a biotin-PEG terminated surface (bottom). The approximate area shown in the image is 14.33 um^2.

Table **3-3**: Summary of streptavidin nano-particle binding experiment on deposited films with modified surfaces.

Surface Modification	Average nano-particle count per SEM image	Average # of nano-particles per um^2
Cysteamine	18	1.25
PEG	1	.07
Biotin-PEG	57	3.98

Once conditions were optimized using the studies above, impedance measurements examined the interaction of both streptavidin and streptavidin coated nano-particles on the electrodes of nano-gap devices modified with the above chemistries. After reacting with streptavidin or streptavidin coated nan-particles, there were little to no changes in device impedance characteristics.

Excellent results were obtained using breakdown curves on modified PtCuPt devices to study the effects of streptavidin nano-particle binding within the device. Prior to breakdown testing on the PEG assembled devices, studies were done to see the effectiveness in simply detecting streptavidin coated nano-particles with the device. On these unmodified devices, electrical biasing was also used to electrically move the beads in and out of the electrode gap. The biasing was done by holding both of the electrodes at ground and biasing a probe which was inserted into the bulk solution.

Figure **3-13** shows breakdown sweep data for three devices that were under different bias conditions during streptavidin nano-particle exposure: one that was not biased, one with a +.1V bias on the probe with respect to the electrodes, and one with a -.1 bias on the probe with respect to the electrodes.

Prior to drying the devices for 20min in a vacuum, a quick rinse in DI water (1min) was performed. This DI rinse step allows salts to diffuse from the nano-channel while not allowing enough time for the nano-particles to diffuse significantly because of their size. This technique, reported for the first time, creates far more reproducible results by eliminating salt crystal and crust formation within the gap. The figure shows a clear difference between the IV characteristics of these devices. The device that did not have bias is expected to contain nano-particles within the gap, because they were carried in to the gap while the device filled. The presence of nano-particles in this case caused an abnormally high current at low voltages. The device with a bias of -.1V also had this low resistive characteristic, again indicating the presence of nano-particles. The device with a bias of .1V did not show these effects and matched a typical curve for a dry device, indicating no presence of nano-particles. The nano-particles were repelled in this case, which agrees with the information provided by British Biocell Inc. that nano-particles prepared in this fashion have a slightly negative charge. The reason for the resistance changes will be further discussed in the next chapter.

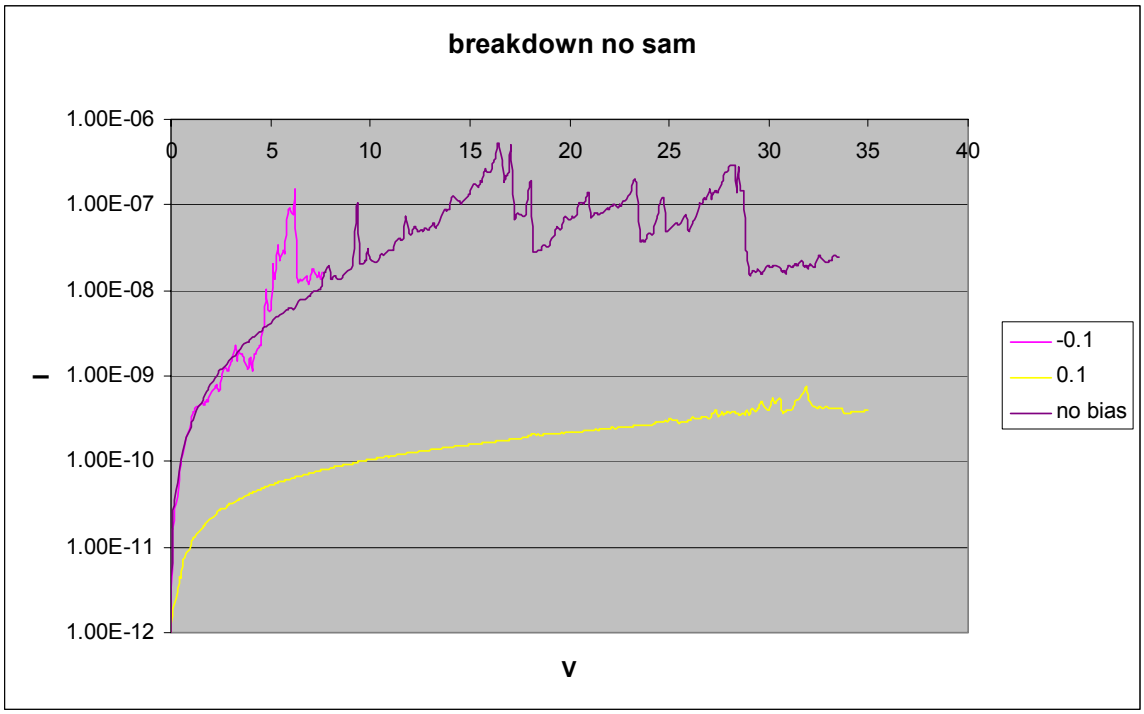

Figure **3-13**: Breakdown sweep results for dry devices under various probe bias conditions during exposure to a streptavidin coated nano-particle solution.

Using the PtCuPt devices with the self-assembling chemistry, the detection of the interaction of the streptavidin coated nano-particles with the biotin-PEG was clearly demonstrated. Here, a PEG and a biotin-PEG modified device were exposed to a streptavidin nano-particle solution, with some devices biased to attract the nano-particles. Results from this experiment are shown in Figure **3-14**. Devices with beads attracted into the gap electically and devices relying on diffusion alone both showed excellent selectivity to streptavidin binding using a breakdown measurement. The resistance difference is not as pronounced as the results above, because the PtCuPt devices were fabricated on aluminosilicate glass with a high background current. Even so, there is

approximately an order of magnitude current difference at low voltages between the devices with biotin-PEG and those with PEG, clearly detecting the presence of streptavidin coated nano-particles bound to the biotin.

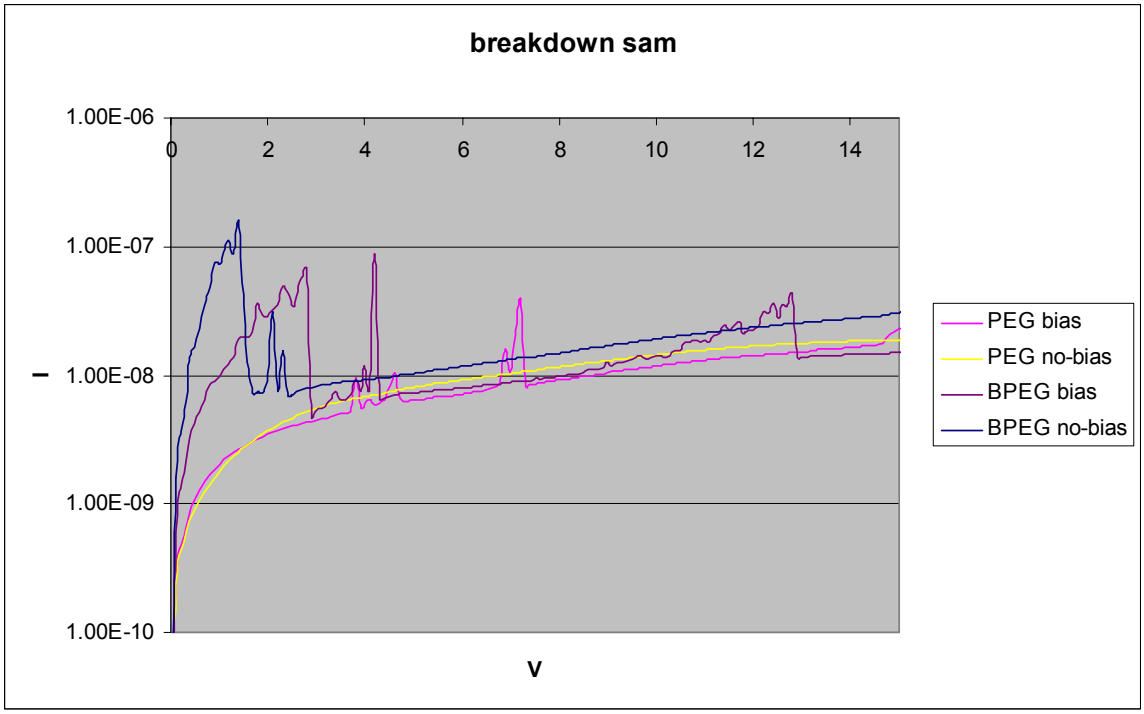

Figure **3-14**: Breakdown sweep results for biotin and non-biotin PEG modified devices which were exposed to streptavidin coated nano-particles under different bias conditions.

3.11 Summary of Results

The results demonstrate the completion of all three of the goals of this work, namely: (1) fabricate an improved device with high strength and chemical functionality, (2) develop selective self assembling chemistry for a biological binding interaction study, and (3) electrically detect the biological interaction

using the improved device. The first time use of a copper sacrificial layer enabled a platinum electrode device to have chemical functionality as confirmed with AC impedance measurements. This platinum device also had excellent dc breakdown characteristics and was able to be used in bead breakdown experiments. The unique two-step PEG-biotin reaction for nano-particle attachment on metal electrodes, developed and demonstrated for the first time in this work, showed excellent selectivity using streptavidin coated nano-particles and SEM analysis. Combining the reaction chemistry and the improved PtCuPt devices, goal number three was clearly achieved using bead breakdown analysis. The biotin-streptavidin binding interaction was also explored using AC measurements on the devices; however, the breakdown experiments showed the best results with an order of magnitude current difference between the presence and absence of the streptavidin nano-particles after the binding experiment.

3.12 References

1. W. J. Nam, “Molecular Scale Gap Sensors Fabricated Using Sacrificial Layers and Self-Assembly,” dissertation, University Park: Penn State University, 2003.

2. A. Ulman, “Formation and Structure of Self-Assembled Monolayers,” Chemistry Reviews, vol. 96, pp.1533-1554, 1996.

3. S. Murarka, Metallization: Theory and Practice for Vlsi and Ulsi, New York, NY,Butterworth-Heinemann,1993.

Chapter 4

Discussion and Analysis of Key Results

This chapter discusses key results presented in Chapter 3, providing an analysis of data and theoretical models to explain various effects. A discussion of results from the various electrode and sacrificial layers used in fabrication will be given along with detailed analysis of certain observations. A circuit model for the device will be presented and used to interpret some of the AC impedance data. Finally, a discussion of the nano-particle breakdown results will be given.

4.1 Electrode and Sacrificial Layer Materials

4.1.1 Gold Electrode Devices

The compositionally graded devices were fabricated to prevent poor adhesion of Au to the adhesion metals in the electrode structure. The devices with graded Au - Ti electrodes had unexpected poor mechanical strength. Optical inspection quickly determined the cause of the poor performance. A picture of the electrode structure is given in Figure **4-1**. This picture shows that the top electrode has an offset of the Ti and Au films. The reason for this offset is explained in Figure **4-2**. The geometrical configuration of the co-evaporation process inherently shifts the position of the two films. This offset would create regions where only gold is adhered to the silicon dioxide surface. The very poor

adhesion of the gold in these areas explains why the breakdown characteristics were so poor.

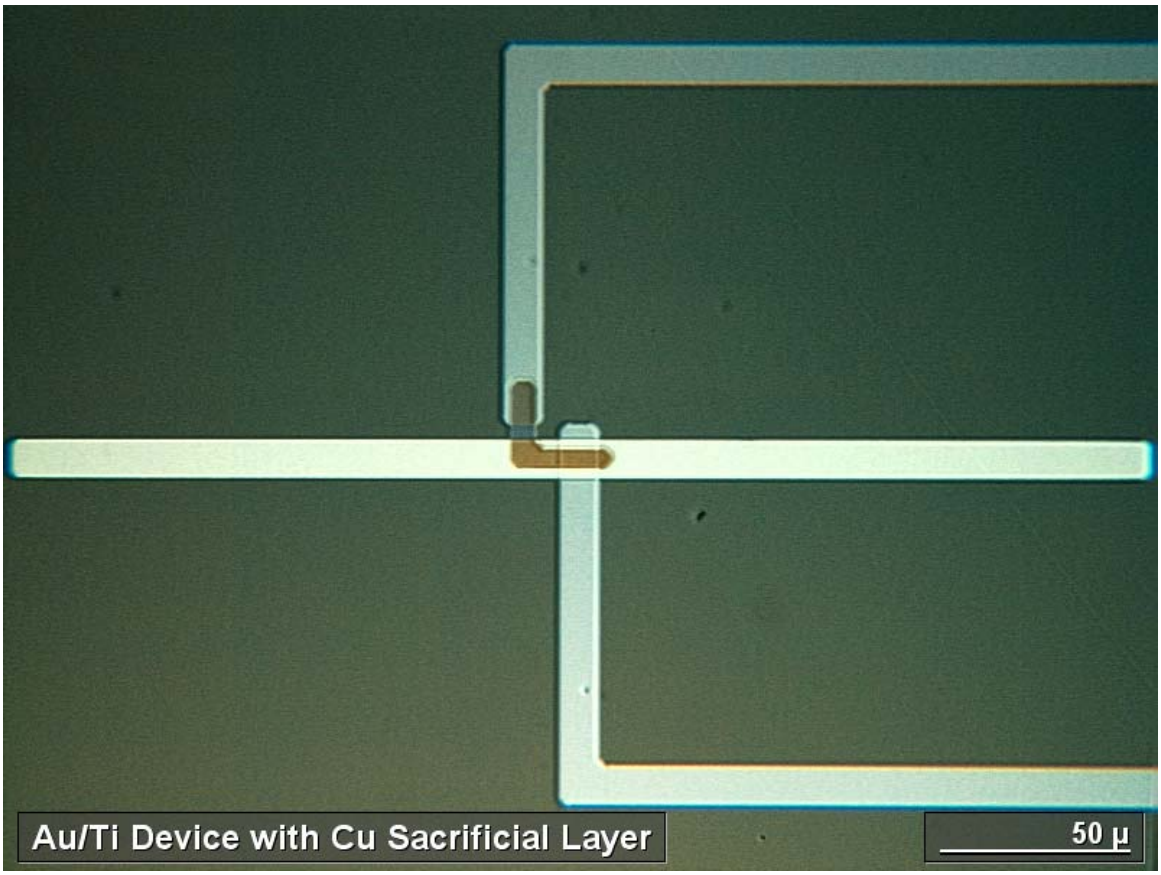

Figure **4-1**: Top-down picture of a device with a graded gold-titanium top electrode.

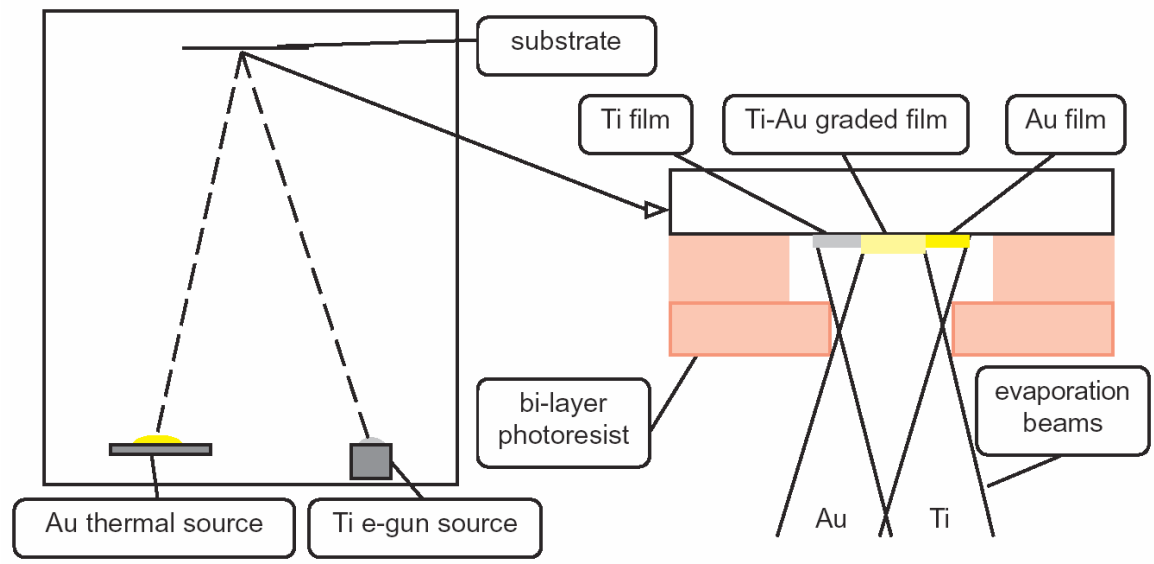

Figure **4-2**: Diagram showing the geometrical configuration of the evaporation system and its effect on a co-evaporated film on a lithographically defined feature.

Another grading scheme was attempted to solve this problem. Here a titanium adhesion layer was deposited, followed by a grading of gold-platinum. The geometrical configuration of this evaporation, shown in Figure **4-3** , ensured that the gold layer was entirely contacted by metal. A small portion of the gold was adjacent to the titanium only, and a small portion of the platinum was on glass only; However, this did not weaken the breakdown voltage, which was high as shown in Table 3-1. Although these devices have good strength, they did not have chemical functionality. Platinum alloys very easily with noble metals like gold, so the surface of the electrode is probably a mixture of gold and platinum, which reacted with the nickel as discussed in Chapter 3, not allowing a thiol-reaction to take place.

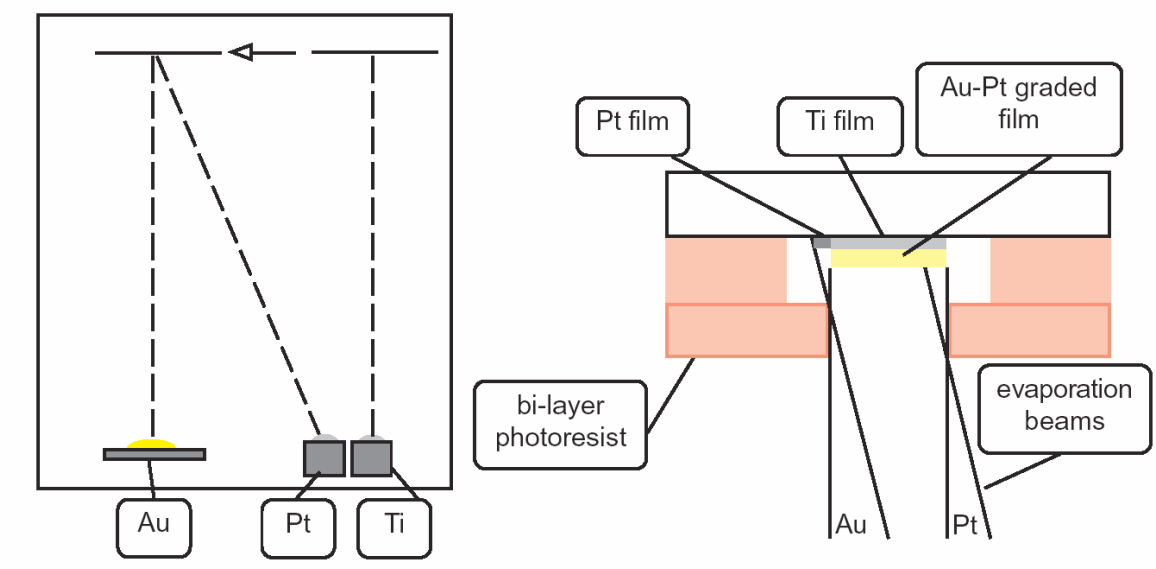

Figure **4-3**: Configuration of a two step graded deposition technique.

4.1.2 Copper Sacrificial Layer Devices

At first, the etchants used in the removal of the sacrificial layer were thought to damage the platinum devices, causing them to be non-functional. Performing experiments on open deposited films, not in a device configuration, showed this to be incorrect (see Table 3-2). Platinum exposure to two nickel etchants, type TFB (nitric acid based) and type I (hydrochloric acid based), does not prevent subsequent thiol-based chemistry on the surface. However, nickel deposited on the surface and then etched away rendered the surface inert to sulfur bonds. The nickel and platinum films alloyed too easily despite attempts to deposit the nickel at different rates to prevent the deterioration of the platinum surface. Palladium was explored as a sacrificial layer, because it dissolves in

nickel etch type I and even if it alloys, is known to form a thiol bond. However, the platinum, once the palladium was removed, also did not show functionality. This is probably due to a chemical modification to the palladium (chlorination) that remains within and exposed on the platinum surface.

Copper as a sacrificial layer proved to be adequate for preserving thiol based functionality after removal from platinum. Alkanethiol mono-layers formed very well on platinum and gold surfaces after removal of the copper layer. As stated in Chapter 3, there was a change in hydrophobicity of the cooper-removed platinum after an alcohol wash. This may be due to the removal of a residual copper surface oxide, which can be reduced with a variety of organic compounds, or the removal of a non-water soluble additive in the etchant mixture. This additive, a perfluoroalky sulfonate molecule, is contained in the nickel type TFB etchant for the purpose of protecting other metals during the etch process.

The difference in device fabrication yield between nickel and copper devices may be due to pitting in the copper sacrificial layer. The copper sacrificial layer is exposed to photoresist remover, high temperature hot-plate steps, photoresist solvents, and photoresist developer prior to the top electrode evaporation. Copper, is a rather corrosive metal and will oxidize very rapidly in atmosphere at mild hotplate temperatures. Its compatibility was tested on the individual chemicals to which it is exposed during processing, and no extensive damage was noted. However, the combination of high temperature steps during lithography (up to 165^{o}C), where the photoresist actually protects the copper

from corrosion, and the TMAH developers caused the copper sacrificial layer to appear slightly “speckled” under high magnification. A microscope picture of this observation with adequate resolution was difficult to obtain. When the copper oxidizes it becomes very rough and does not maintain a smooth finish. Therefore, this slight oxidation due to processing conditions may create a rough surface and pitting of the film. This damaged sacrificial layer allows the formation of shunts between the electrodes in some of the devices, causing yield loss.

4.2 Impedance Circuit Models

Circuit models for the device provide insight into the impedance characteristics of the device and the changes observed with self-assembly experiments. The device is essentially a parallel plate capacitor, but the circuit model becomes complex when the inter-electrode regions becomes filled with liquids. In addition, there are parasitic effects as observed in Chapter 3. As shown below, even as a simple capacitor, the device impedance characteristics are difficult to model exactly.

A simple circuit model for the device in an air state is shown in Figure **4-4**. Here, the capacitor corresponds to the air-gap capacitor formed by the electrodes and the resistor is a sum of the possible leakage resistances including among others, conduction through mobile silicon dioxide defects including charge, mobile surface charge in the nano-channel (residual water), and

ionization events in the air-gap. The series resistance and parasitic capacitance from the leads is eliminated through calibration of the impedance analyzer.

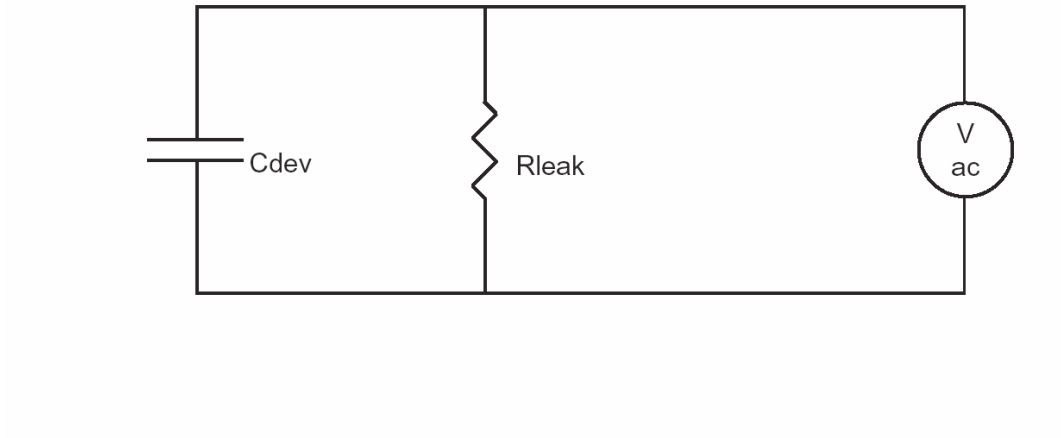

Figure **4-4**: Circuit model of the air state of the nano-gap device. Cdev is the nano-gap structure capacitance, and Rleak is leakage resistance from a sum of possible sources.

A plot of the calculated and measured impedance of the air-state of the device is given in Figure **4-5**. The measured and model reactance curves match very well with a capacitance value of 60fF, which is not unreasonable when compared to a calculated value of 13fF based on measured dimensions. Fringe effects and electrode roughness contribute to the higher measured capacitance. The resistance curves shown in Figure **4-5** however, do not agree well with what is expected. The model shown uses a resistor value of 1Gohm. Surprisingly, adding elements to the simple circuit model above does not help to match the slope of the resistance curve. Although it is unclear why it occurs, the parallel resistor element appears to have frequency dependant resistance. To match the

resistance curve shown in the figure, the resistor would have to drop from 1Gohm to 10Mohm going from 10kHz to 1MHz.

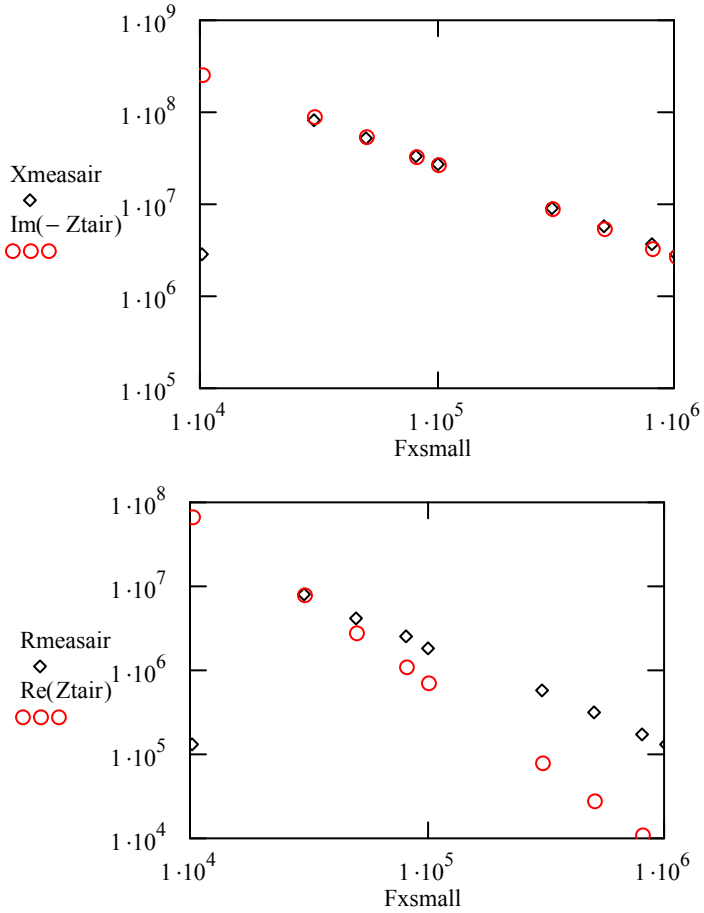

Figure **4-5**: Measured (black diamonds) and theoretical (red circles) impedance values of a device versus frequency in an air gap state. (top) Reactance and (bottom) Resistance

This model can be used to explore the impedance characteristics of a partially dry device shown in Figure 3-6. To match the impedance curves of the partially dry device, the only modification to the above model is to change the leakage resistance to 6.5 Gohms. Impedance curves are shown in Figure **4-6**. Physically, the change in impedance characteristics is probably due to water, not

present between the electrodes, but in the nano-channel, creating a current path along the channel to the two electrodes. If water was between the electrodes, the capacitor value would need to also change, which it does not. Although the applied voltage of 50mV is too low to cause electrochemical reactions on the platinum electrodes, the reduced resistance indicates that these reactions are occurring. They may be occurring on exposed portions of the Ti adhesion layer.

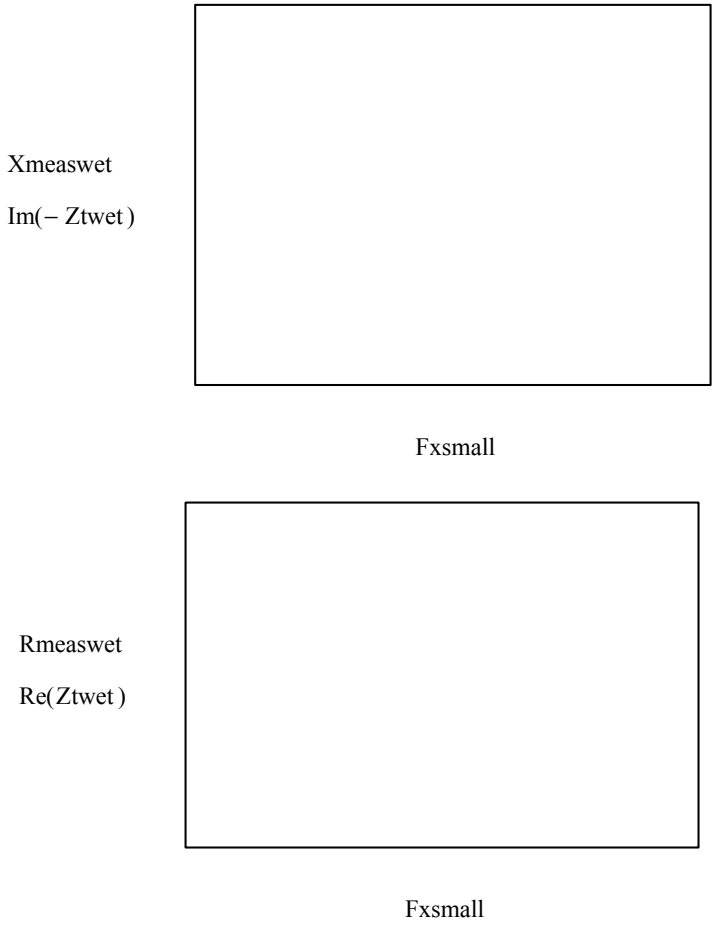

Figure **4-6**: Measured (black diamonds) and theoretical (red circles) impedance values of a device versus frequency in a partially dry device state. (top) Reactance and (bottom) Resistance

When the nano-gap devices are filled with an electrolytic liquid their impedance characteristics become very complicated. When an electrolytic liquid enters the gap, electrical double layers form on the electrodes (compact and diffuse layers) adding capacitors at the electrode surfaces to the circuit model. Also, the relative dielectric constant of the liquid (80 for water) increases the geometrical device capacitance. A circuit model is shown in Figure **4-7**.

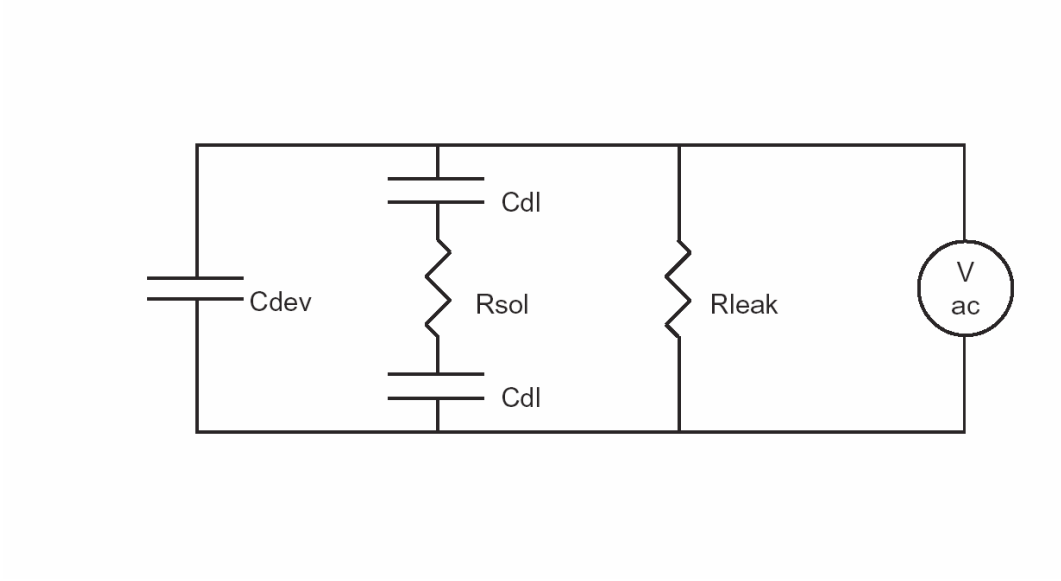

Figure **4-7**: Circuit model of the electrolyte filled state of the nano-gap device. Cdev is the nano-gap structure capacitance, and Rleak is leakage resistance from a sum of possible sources. Cdl is the double layer capacitance and Rsol is the resistance of the electrolyte solution.

Using the values optimized above and estimated values for the double layer capacitance and solution resistance, the theoretical impedance characteristics are shown in Figure **4-8**. Here, the resistance and reactance curves do not match at high frequencies, again indicating a frequency

dependence of one of the circuit elements. Also the low frequency impedance is incorrect, most probably because of parasitic elements.

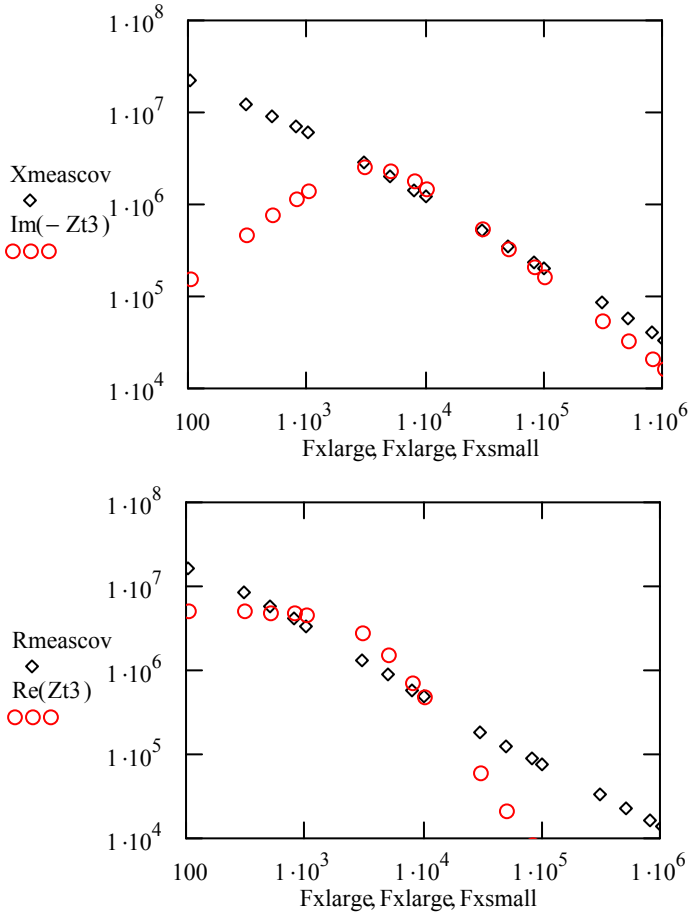

Figure **4-8**: Measured (black diamonds) and theoretical (red circles) impedance values of a device versus frequency in an electrolyte solution. (top) Reactance and (bottom) Resistance

In the low frequency range, parasitic leakage resistances and capacitances dominate. As an example, Figure **4-9** shows how decreasing the leakage resistance effects the impedance characteristics. This gives insight into the curves taken in Figure 3-5; i.e., increasing the electrode exposure to the liquid causes the impedance parameters to change.

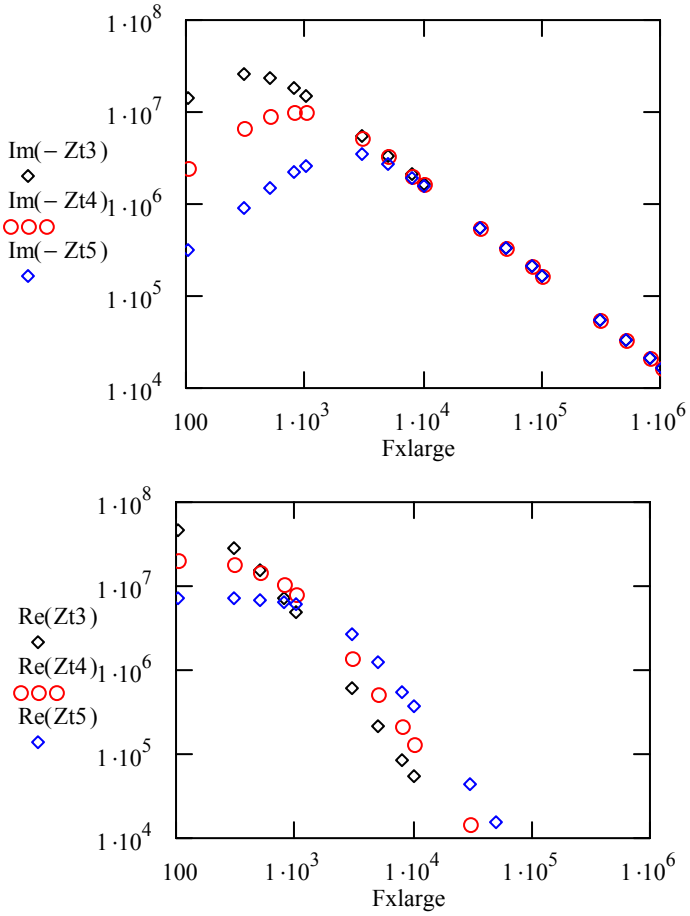

Figure **4-9**: Impedance model showing the effect of increasing leakage resistance. Rleak = 50Gohms (black diamond) 20Gohms (red circle) and 7Gohms (blue diamond) (top) Reactance and (bottom) Resistance

Interpreting the impedance data from the self-assembled monolayer experiments is difficult. It has been shown that self-assembled monolayers of alkanethiols push back the ions in the helmholtz layer reducing the capacitance [**1**]. This occurs in the self-assembly experiments in Section 3-2-2-2. The increase in reactance corresponds to a decrease in capacitance (X=1/jWC). A curious result is the PEG assembly, where the reactance decreases, increasing the capacitance. It is not known at this time why this occurs. The only other

observation of increased capacitance occurs when the device is exposed to a salt solution for extended periods, corroding and increasing the surface are area of the electrodes.

4.3 Nano-Particle Breakdown Results

A technique using breakdown current-voltage sweeps identified the presence of nano-particles within the nano-gap sensor device, detecting the binding of biotin to streptavidin coated on the nano-particle surface. The nano-particles caused a large increase in the air-state (dry) conductivity of the device as shown in Figures 3-13 and 3-14.

The change in the I-V characteristics looks very similar to a device that is not dry fully in the nano-channel (see Figure 3-3), indicating that the presence of nano-particles might change the device drying time, or retain water. However, several factors point to a different model. First, some of the devices showed an increase in resistance until high voltages, such as the no-bias device in Figure 3-13. A wet device quickly hydrolyzes the water present in the nano-channel and resumes to the original device conductivity. Furthermore, the high-conductivity curves due to nano-particles are repeatable, meaning that the device, if not broken, can be biased again, showing the same conductivity. Wet-channel devices return to their original characteristics once dry after a single sweep.

The high conductivity observed due to the presence of nano-particles is probably due to combination of effects, depicted in Figure **4-10** . In the high

fields present during voltage sweeps, arcing between nano-particles and the electrodes is likely. This will contribute to current fluctuations and probably cause nano-particles to melt and fuse together with each other and the electrodes. This helps to explain the noisy current fluctuations seen in the data. Also, given the small distances between conducting particles and surfaces, a contribution due to tunneling current is possible. Assembled beads may also act to bridge the gap and form residual conductive pathways as shown in the figure. Even though all surfaces may be coated with insulating layers, conducting surface pathways will be formed. Regardless of the exact mechanism by which this technique works, it shows great promise and rationale for furthering the work and specifically exploring its commercial potential and development.

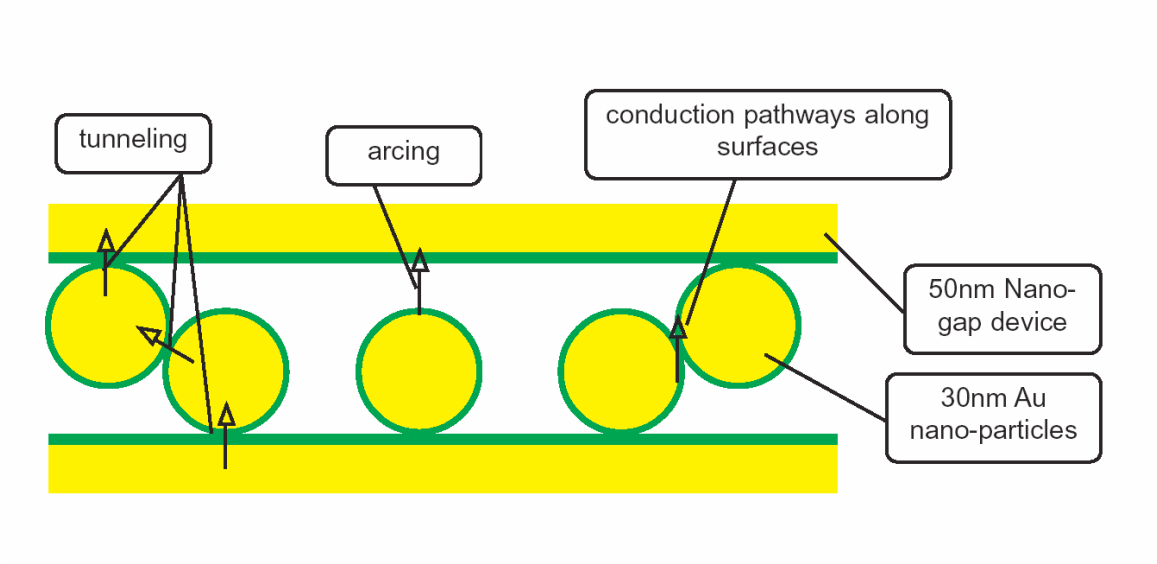

Figure **4-10**: Schematic of current pathways created with the presence of nano-particles within the nano-gap sensor.

4.4 Reference

1. A. Bard and L. Faulkner, Electrochemical Methods, John Wiley & Sons Inc.,pp.534-580,2001.

Chapter 5

Conclusions and Future Work

This thesis presents novel developments in the fabrication and use of a nano-scale gap sensor which advance the field of electrical bio-molecular sensing. This work has achieved the three goals presented in Chapter 1, namely: 1) to fabricate a nano-gap device with combined high strength and chemical functionality, 2) to develop self-assembling chemistries on metals to test and evaluate bio-molecular sensing within the nano-gap structure, and 3) to demonstrate electrical detection of the interaction of bio-molecular species with the improved device and electrode surface chemistry. The following sections review the results in light of these three goals and make conclusions as to the practicality of the device for commercial use. Suggestions for future work also follow.

5.1 Improved Device Fabrication

The realization of an electrode/solution/electrode device configuration with high strength and the ability to chemically tailor the surface of the electrodes is very important for this device to be useful as a bio-sensor. The ability to chemically attach organic species to the electrodes is a fundamental necessity for the device to interact with biological species. The high strength is necessary

also in order for the device to withstand experimental handling and the rigors of electrical measurements. Such strength is very necessary for testing voltage breakdown measurements for the detection of the presence of species. Our group's prior work demonstrated a Pt electrode device with high strength but poor chemical attachment ability and an Au electrode device with poor strength but good chemical attachment ability [**1**]. This thesis presents, for the first time, a device with the combination of high strength and good chemical attachment ability. This has been achieved by using a Cu sacrificial layer for Pt electrode devices. These devices have a breakdown voltage of 28V and are robust during handling. The chemical functionality of the electrodes was confirmed using self-assembling chemistry and impedance measurements as described in Section 3.2.2.2.

These unique devices are not only useful for the biological detection schemes presented in this thesis, but are also useful in improving the work of other groups. For example, the electrical bridge techniques presented by [**2**] and [**3**], reviewed in Chapter 1, are limited in sensitivity and detectable length of DNA by the distance of their inter-electrode gap. Or sensor and fabrication techniques offer a nanometer scale electrode structure that is robust and chemically functional, improving the sensitivity of the bead-based technique [**2**] and the allowing small strands of DNA to be detected for the DNA plating technique [**3**].

The fabrication of the nano-scale gap device presented in this thesis uses typical cost-effective semiconductor processes. However, the step of depositing a 10um capping layer of silicon dioxide may not meet commercial cost

requirements because of the long deposition times (8 hrs) associated with the step. Results obtained during this work, provide insight on how to improve the capping layer process. It was shown that only a 4um silicon dioxide provides for a robust device but not for enough electrical insulation. Future work for commercial development may include a two step capping layer process, where a thin silicon dioxide layer is deposited first for mechanical stability and then a spin on dielectric is applied second for electrical insulation.

Device yield is also important to gauge the robustness of the process flow used to fabricate these unique devices. The device yield for the Cu sacrificial layer devices is currently 75%. The corrosion of the Cu sacrificial layer during processing, as discussed in Section 4.1.2, is the most probable cause for the imperfect yield. Fine tuning the process flow to eliminate Cu sacrificial layer damage should be performed to realize commercial production of these devices. Otherwise, the majority of the steps in the process flow are ready, as they stand, for commercial manufacturing.

5.2 Improved Self-Assembling Chemistry and Biological Assay

This thesis presents a unique surface chemistry which allows for the immobilization of active biological species on an electrode surface. This surface chemistry includes the use of a PEG polymer spacer between the surface of the metal and the attached bio-molecule, biotin in this case. The spacing allowed streptavidin coated nano-particles to interact with the biotin and attach, and

thereby be tethered to the surface by the PEG chain. The PEG also reduced non-specific binding of streptavidin as shown in Figure 3-12 and Table 3-3. The 50:1 selectivity of the bound streptavidin nano-particles over the control shows that this is an effective scheme and is appropriate for evaluating the nano-gap device as an electrical bio-molecule sensor.

The immobilization of the bio-molecule biotin on the electrode surface was presented in this thesis. This molecule is a small organic molecule which interacts with proteins. The attachment scheme presented in this thesis is not limited to only this type of molecule. Proteins, such as streptavidin, can also be attached to the surface using the PEG spacer concept with small changes in the chemical reaction steps. This allows the electrode modification to be much more general and versatile, enabling a variety of bio-molecular interaction experiments. This is important because any commercial platform will be more useful if the basic structure can be used for a variety of bio-molecular species. Future work here may include exploration of the attachment of other types of bio-molecules and optimization of the various chemistries.

5.3 Electrical Detection of Bio-Molecular Interactions

The final goal in this thesis was to use the improved device and improved surface chemistry to detect a bio-molecular reaction electrically. This was achieved using the new Pt devices with a Cu sacrificial layer, using the improved surface chemistry, and using an electrical breakdown technique to detect the

presence of streptavidin coated nano-particles. The results presented in Section 3.2.4 show an order of magnitude difference in current during a voltage sweep between the device with immobilized biotin and the control. The device with the immobilized biotin captured the streptavidin coated nano-particles, and this was shown to be fully detectable with a current change. This is the first time this detection technique has been successfully demonstrated.

The performance of the device as an electrical sensor in this fashion is acceptable for a commercial sensor. An order of magnitude difference in current is more than adequate for analysis with an electrical analysis system. The results obtained in Section 3.2.4 also indicate that higher differences in current levels during detection are possible by using a well-insulating quartz substrate to reduce background current. It is difficult to know the ultimate sensitivity of this device and detection means at this point. However, using the SEM images in Figure 3-12, it can be estimated that the amount of nano-particles contained within the electrode gap is on the order of 150 nano-particles. Given that there are approximately 80 streptavidin molecules attached to each nano-particle, the amount of streptavidin effectively detected is approximately 12,000 molecules. Other groups have boasted detection limits of 30,000 [**4**] and 40,000 [**5**] molecules, and to the authors knowledge, our results are the best detection limits reported for the electrical detection of a bio-molecular interaction.

5.4 References

1. W. J. Nam, “Molecular Scale Gap Sensors Fabricated Using Sacrificial Layers and Self-Assembly,” dissertation, University Park: Penn State University, 2003.

2. S. Park, T. A. Taton, and C. A. Mirkin, “Array-Based Electrical Detection of DNA with Nanoparticle Probes,” Science, vol. 295, pp. 1503-1506, 2002.

3. E. Braun, Y. Eichen, U. Sivan, and G. Ben-Yoseph, “DNA-Templated Assembly and Electrode Attachment of a Conducting Silver Wire,” Nature, vol. 391, pp. 775-778, 1998.

4. J. Wang, R. Polsky, A. Merkoci, and K. L. Turner, ““Electroactive Beads” for Ultrasensitive DNA Detection,” Langmuir, vol. 19(4), pp.989-991, 2003.

5. D. J. Caruana and A. Heller, “Enzyme-Amplified Amperometric Detection of Hybridization and of Single Base Pair Mutation in an 18-Base Oligonucleotide on a 7-um-Diameter Microelectrode,” Journal of the Americal Chemical Society, vol. 121, pp. 769-774, 1999.

JOSEPH DENNIS CUIFFI

Current Address
7850 Reflection Cove Drive, Apt 202
Fort Myers, FL 33907
(814) 404-1261, jdc167@psu.edu

Permanent Address
31 Falkirk Drive
Pittsburgh, PA 15235
(412) 793-0574

OBJECTIVE My research focuses on the integration of nanotechnology into devices and materials for biological and chemical sensors and systems.

EDUCATION

Ph. D. candidate, Penn State Engineering Science & Mechanics (GPA: 3.8)
Emphasis: Education and research encompassing the integration of material science and nano-fabrication with chemical and biological systems.
UNDERGRADUATE
Bachelor of Science in Engineering Science with Honors (GPA: 3.95/3.95)
The Pennsylvania State University, May 1999
Honors Thesis: "A Novel Approach to Diode PROM Using a Directional Breakdown of Amorphous Silicon," Advisor: Dr. Stephen J. Fonash

TECHNICAL WORK HISTORY

Research and Development, NanoHorizons Inc.
January 2001-present – Co-founder, currently developing products in the fields of biotechnology and micro-electronics
Graduate Research Assistant, Penn State Department of Engineering Science
May 1999-present - Conduct research in the area of biological and chemical integration with materials, nano-fabricated devices and detection schemes, plus semiconductor device modeling, and novel nano-fabrication techniques
Research Intern, Argonne National Laboratory
May 1998-August 1998 - Internship opportunity at the INEEL nuclear reactor site which involved nuclear reactor simulations, their use in nuclear waste transport design, and building a data acquisition system.

SELECT PUBLICATIONS & PRESENTATIONS

"Analysis of the Effects of Nanostructured Thin Film Morphology and Surface Chemistry on Cell Adhesion," submitted to BioMEMS & Biomedical Nano Technology World 2001, September 22, 2001.
"Desorption-ionization Mass Spectrometry using Deposited Nanostructured Silicon Films," Analytical Chemistry 73 (6), March 15, 2001.
"Nanostructured Silicon for Bio-Medical Applications," Proceedings of SPIE - The International Society for Optical Engineering, Smart Electronics and MEMS II, December 15, 2000.
"A Trapped Charge Model for the Transient Effect in CIGS Solar Cells," presented and published at the Photovoltaic Specialists Conference, September 15, 2000.

HONORS

Dean's Fellowship
August 1999 – May 2002
The Evan Pugh Junior Scholar Award
April 1998, Honors award distinguishing the top five percentile of the class